Enhancer AAV toolbox for accessing and perturbing striatal cell types and circuits

Authors
Avery C. Hunker[1,#], Morgan E. Wirthlin[1,#], Gursajan Gill[2], Nelson J. Johansen[1], Marcus Hooper[1], Victoria Omstead[1], Naz Taskin[1], Natalie Weed[1], Sara Vargas[1], Jacqueline L. Bendrick[2], Bryan Gore[1], Yoav Ben-Simon[1], Yeme Bishaw[1], Ximena Opitz-Araya[1], Refugio A. Martinez[1], Sharon Way[1], Bargavi Thyagarajan[1], M. Nathaly Lerma[1], Will Laird[1], Otto Sven[1], Raymond E.A. Sanchez[1], Jason R. Alexander[1], Avalon Amaya[3], Adam Amster[1], Angela Ayala[1], Pam M. Baker[1], Tyler Barcelli[1], Stuard Barta[1], Darren Bertagnolli[1], Cameron Bielstein[1], Prajal Bishwakarma[1], Jessica Bowlus[1], Gabriella Boyer[1], Krissy Brouner[1], Brittny Casian[1], Tamara Casper[1], Anish Bhaswanth Chakka[1], Rushil Chakrabarty[1], Michael Clark[1], Kaity Colbert[1], Scott Daniel[1], Tim Dawe[1], Maxwell Departee[1], Peter DiValentin[1], Nicholas P. Donadio[1], Nadezhda I. Dotson[1], Deepanjali Dwivedi[1], Tom Egdorf[1], Tim Fliss[1], Amanda Gary[1], Jeff Goldy[1], Conor Grasso[3], Erin L. Groce[1], Kathryn Gudsnuk[1], Warren Han[3], Zeb Haradon[1], Sam Hastings[1], Olivia Helback[1], Windy V. Ho[1], Cindy Huang[1], Tye Johnson[3], Danielle L. Jones[1], Zoe Juneau[1], Jaimie Kenney[3], Madison Leibly[1], Su Li[1], Elizabeth Liang[1], Henry Loeffler[3], Nicholas A. Lusk[1], Zachary Madigan[1], Jessica Malloy[1], Jocelin Malone[1], Rachel McCue[1], Jose Melchor[1], John K. Mich[1], Skyler Moosman[1], Elyse Morin[1], Robyn Naidoo[3], Dakota Newman[1], Kiet Ngo[1], Katrina Nguyen[3], Aaron L. Oster[1], Ben Ouellette[3], Alana A. Oyama[1], Nick Pena[1], Trangthanh Pham[1], Elliot Phillips[1], Christina Pom[1], Lydia Potekhina[1], Shea Ransford[1], Melissa Reding[1], Dean F. Rette[1], Cade Reynoldson[1], Christine Rimorin[1], Ana Rios Sigler[1], Dana B. Rocha[1], Kara Ronellenfitch[1], Augustin Ruiz[1], Lane Sawyer[1], Josh Sevigny[1], Nadiya V. Shapovalova[1], Noah Shepard[1], Lyudmila Shulga[1], Sherif Soliman[1], Brian Staats[1], Michael J. Taormina[1], Michael Tieu[1], Yimin Wang[1], Josh Wilkes[3], Toren Wood[1], Thomas Zhou[1], Ali Williford[3], Nick Dee[1], Tyler Mollenkopf[1], Lydia Ng[1], Luke Esposito[1], Brian Kalmbach[1,4], Shenqin Yao[1], Jeanelle Ariza[1], Shoaib Mufti[1], Kimberly Smith[1], Jack Waters[1], Ina Ersing[5], Marcella Patrick[5], Hongkui Zeng[1], Ed S. Lein[1,6], Yoshiko Kojima[7,8], Greg Horwitz[4,8], Scott F. Owen[2], Boaz P. Levi[1], Tanya L. Daigle[1,4], Bosiljka Tasic[1], Trygve E. Bakken[1], Jonathan T. Ting[1,4,8^]

[1]Allen Institute for Brain Science, Seattle, WA
[2]Department of Neurosurgery, Stanford University School of Medicine, Stanford, CA
[3]Allen Institute for Neural Dynamics, Seattle, WA
[4]Department of Neurobiology & Biophysics, University of Washington, Seattle, WA
[5]Addgene Watertown, MA
[6]Department of Neurological Surgery, University of Washington, Seattle, WA
[7]Department of Otolaryngology, Head and Neck Surgery, University of Washington, Seattle, WA
[8]Washington National Primate Research Center, Seattle, WA
[#]Equal contribution
^Lead Contact

Correspondence: JonathanT@alleninstitute.org

Keywords
Medium spiny neuron, spiny projection neuron, cholinergic, Sst-chodl, Pvalb, basal ganglia, caudoputamen, Adeno-associated virus, Addgene, striatonigral, striatopallidal

Abstract
We present an enhancer AAV toolbox for accessing and perturbing striatal cell types and circuits. Best-in-class vectors were curated for accessing major striatal neuron populations including medium spiny neurons (MSNs), direct and indirect pathway MSNs, as well as Sst-Chodl, Pvalb-Pthlh, and cholinergic interneurons. Specificity was evaluated by multiple modes of molecular validation, three different routes of virus delivery, and with diverse transgene cargos. Importantly, we provide detailed information

necessary to achieve reliable cell type specific labeling under different experimental contexts. We demonstrate direct pathway circuit-selective optogenetic perturbation of behavior and multiplex labeling of striatal interneuron types for targeted analysis of cellular features. Lastly, we show conserved *in vivo* activity for exemplary MSN enhancers in rat and macaque. This collection of striatal enhancer AAVs offers greater versatility compared to available transgenic lines and can readily be applied for cell type and circuit studies in diverse mammalian species beyond the mouse model.

Introduction

The striatum, a key component of the basal ganglia, plays a critical role in motor control, habitual behaviors, and cognitive functions, and its dysfunction is central to a variety of movement disorders and substance use disorders[1–4]. The striatum is comprised of diverse neuronal populations, including the highly abundant medium spiny neurons (MSNs) and relatively rare local interneurons, each contributing important roles within functionally distinct circuits[5–8]. MSNs are the GABAergic projection neurons of the striatum and are divided roughly equally between Drd1 and Drd2 receptor expressing neuron subtypes (D1 MSNs and D2 MSNs, respectively). Effective targeting and manipulation of these distinct cell types is crucial for unraveling their specific contributions to functional circuits and for developing effective therapeutic interventions to treat basal ganglia disorders.

Considerable progress has been made with respect to delineating cellular and synaptic properties and dissecting the functional role of distinct striatal cell types to mouse behavior. This rapid progress has largely been attributable to the development of transgenic mouse lines, used alone or in combination with viral labeling strategies, to achieve reliable genetic targeting and perturbation of striatal circuit components. For example, cell type-specific bacterial artificial chromosome (BAC) transgenic GFP reporter and Cre driver lines from the Gene Expression Nervous System ATlas (GENSAT) project (www.gensat.org)[9] provided a means by which researchers could directly test foundational circuit models about the role of the so-called direct (striatonigral) versus indirect (striatopallidal) basal ganglia pathways in motor initiation, coordination, and dysfunction. Drd1-GFP and Drd1-Cre BAC transgenic lines were initially developed for targeting direct pathway D1 MSNs, and Drd2-GFP and Drd2-Cre lines for targeting indirect pathway D2 MSNs[10,11]. Many other derivative BAC transgenic mouse lines followed, offering improved specificity of labeling (e.g., Adora2a-Cre[9]) or alternate transgene cargos (e.g., D1 and D2 BAC trap lines[12] or Drd1a-tdTomato line[13]) for diversifying experimental applications. Similarly, various other transgenic mouse lines have been utilized to target the diverse interneuron types of the striatum, often with cell type discrimination based on a combination of distinctive neurochemical, morphological, and electrophysiological signatures[6,14,15].

Importantly, none of the foundational transgenic mouse lines mentioned above are applicable for research in other species. AAV vectors paired with compact cell type-specific enhancers can offer a promising alternative to mouse transgenic technologies to bridge this important gap and to enable genetic targeting of homologous cell types both in the mouse and across additional mammalian model species. Notably, enhancer AAVs can be used in wild-type animals and do not require complicated breeding of transgenic mouse lines. We and others have demonstrated feasibility of enhancer AAVs for targeting diverse cortical neuron types in mice, rats, ferrets, marmosets, macaques, and human *ex vivo* brain slices derived from neurosurgeries[16–26]. Notably, cell type specific enhancer discovery is directly enabled by emerging large-scale single cell epigenetic datasets, especially single cell (sc) and single nucleus (sn) Assay for Transposase Accessible Chromatin with sequencing (sc/snATAC-seq), aligned to brain cell type taxonomies from sc/snRNA-seq. Foundational striatal cell type taxonomies are currently available to compare and align for the mouse[27–30], marmoset[31], macaque[32], and human[33,34], and serve as a foundational transcriptomic framework for future viral genetic tool molecular validation and use for biological discovery.

Our study aimed to develop and validate an enhancer AAV toolbox for targeting several major striatal neuron populations, including pan-MSNs, direct and indirect pathway MSNs, and Sst-Chodl, Pvalb-Pthlh, and cholinergic interneurons. Using enhancer elements derived from bulk and single-cell ATAC-seq data, we engineered AAV vectors that demonstrate high specificity in labeling these neuronal populations in the mouse brain, with molecular validation anchored in the Allen Institute mouse whole brain hierarchical cell type taxonomy at subclass resolution. We evaluated these vectors for their strength and specificity through various routes of administration and functional assays, including the use of Cre recombinase, opsins, and genetically encoded calcium indicators. Moreover, we investigated suitability of these enhancer AAV vectors for cross-species applications by comparing *in vivo* chromatin accessibility for select MSN enhancers across mouse, rat, and human, and conducting *in vivo* characterization of enhancer AAV activity in rat and macaque brain. The high conservation of enhancer activity across species underscores the immense potential of these tools for new directions in comparative cellular neuroscience and translational research.

The enhancer AAV screening and validation data from this collection can be viewed in the Allen Institute Genetic Tools Atlas (GTA) at https://portal.brain-map.org/genetic-tools/genetic-tools-atlas, an open access community resource created with the support of the NIH BRAIN Armamentarium consortium.

Results

Identification and *in vivo* validation of striatal subclass specific enhancers from diverse epigenetic datasets

To create a striatum-centric enhancer AAV toolbox, we adopted a one-at-a-time screening pipeline evaluating putative enhancer sequences for driving brain region and cell type-specific SYFP2 reporter expression (**Figure 1**). First, promising ATAC-seq peaks were identified proximal to striatal cell type marker genes (**Figure 2A**) in multiple previously published and publicly available human and mouse bulk ATAC-seq datasets (**Figure 2B**). The majority of these enhancers were selected from the human Brain Open Chromatin Atlas (BOCA[35]) and mouse Cis-element ATlas (CATlas[36,37]) as sequences with relatively strong brain region or cell type selectivity in chromatin accessibility (**Figure 2C-D**). An additional handful of enhancer candidates were selected from mouse cortical scATAC-seq data[21] or from a published human M1 dataset[20]. These enhancers were found to exhibit useful cell type specificity in the striatum region in addition to cortex based on prior brain wide expression analysis. Additionally, virtually none of the selected enhancers exhibited accessibility in human tissues outside of the brain (**Figure S1**).

Candidate enhancer sequences were PCR amplified from mouse or human genomic DNA and cloned into an AAV vector upstream of a minimal promoter sequence (either minimal beta globin or minimal Rho promoters) and the bright monomeric SYFP2 fluorescent reporter transgene[38]. Completed vectors were packaged into functional AAV particles using the mouse blood brain barrier penetrant capsid PHP.eB[39] and injected retro-orbitally (RO) into adult wildtype C57Bl6/J mice. At 3-5 weeks post injection the mouse brains were collected for analysis of native SYFP2 reporter expression pattern in the brain.

As striatal medium spiny neurons (MSNs) make up ~95% of all striatal neurons and are defined by their axon projection targets[40,41], D1 MSN and D2 MSN selective labeling was easily identifiable in mid-sagittal brain sections as dense SYFP2^{+} striatal neuron labeling with axons projecting predominantly to the GPi/SNr or GPe, respectively (**Figure 2E**). Similarly, pan-MSN labeling was revealed as dense SYFP2^{+} striatal neuron labeling with axons projecting to both direct and indirect pathway target structures. Several of the MSN enhancers illustrated intra-striatal regional biases, with cell body

expression mostly restricted to either dorsal or ventral striatum (**Figure S2**). In contrast, enhancers that labeled local interneuron populations exhibited SYFP2 fluorescence restricted to the striatum proper and had clearly distinguishable morphological characteristics (**Figure 2F-G**)[5,14,42–44]. Striatal Pvalb-Pthlh interneurons have small round or rectangular somata with compact multipolar aspiny dendrites, cholinergic interneurons have unusually large cell bodies with thick aspiny dendrites, and Sst-Chodl interneurons have elongated small to medium size somata with wispy, thin dendrites.

Following initial evaluation by native SYFP2 fluorescence, we sought to improve enhancer-driven transgene expression by inserting multiple copies of the "core" enhancer region in tandem. This strategy has been previously shown to improve strength of expression while preserving specificity[21,45]. We designed and screened an additional 13 of these "synthetic" enhancers that resulted in stronger SYFP2 fluorescence compared to the original full-length enhancers (**Figure S3**).

Based on analysis of the striatum and brain wide expression patterns, we curated a set of 48 enhancer AAV vectors with promising activity spanning these major striatal neuron populations. This resulted in a collection of 20 pan-MSN enhancers, 5 D1 MSN enhancers, 7 D2 MSN enhancers, 5 Sst-Chodl interneuron enhancers, 7 cholinergic interneuron enhancers, and 4 Pvalb-Pthlh interneuron enhancers (**Figure 2B and S3**). Most enhancers in this set showed high selectivity for the striatum, with minimal or no SYFP2$^+$ cell labeling detected in other brain regions. In the case of Sst-Chodl or Pvalb enhancers we observed labeled neurons in both cortex and striatum regions.

Comparison of strength and specificity of validated striatal MSN enhancers

In the case of enhancer selection based on bulk human ATAC-seq data from BOCA, putative D1 MSN or D2 MSN enhancer candidates were inferred based on proximity to known direct and indirect pathway MSN marker genes (e.g., *Drd1* and *Drd2*). Additional criteria included differential chromatin accessibility in striatum neuronal samples versus all other brain region neuronal samples including multiple cortex regions, thalamus, hippocampus, and amygdala. Because the source epigenetic data used for selection did not have the resolution of subclasses we were targeting, we found that some enhancers inferred as putative D1 MSN or D2 MSN enhancers instead yielded pan-MSN reporter activity that was nonetheless fully consistent with the bulk epigenetic signatures.

To explore the relative strength of a set of validated pan-MSN enhancers, we designed a multiplex experiment to directly compare the enhancers in the mouse brain *in vivo* (**Figure S4A**). We chose to include twelve pan-MSN enhancers as well as one D1 MSN enhancer and one D2 MSN enhancer to confirm our ability to resolve subclass specific labeling. An 8-base pair (bp)-barcode was cloned between the WPRE3 and bGHpA of each parental enhancer AAV construct, packaged separately into PHP.eB and administered RO into an adult mouse as a single pooled injection. SYFP2$^+$ whole cells were collected via FACS and used to generate 10x v3.1 single cell gene expression and AAV transcript (barcode) libraries. Enhancer specificities were determined by the presence of AAV barcode following mapping of sequenced libraries to the mouse whole brain taxonomy (see **Methods** for details).

We examined properties that reflect enhancer cell type specificity, strength, and broadness of labeling across the striatum. We did not observe any major differences in cell type specificity, as almost all pan-MSN enhancer AAVs labeled equivalent proportions of D1 and D2 MSNs (STR D1 Gaba and STR D2 Gaba in the taxonomy). The exception was AiE0450h which exhibited a STR D2 Gaba bias, which is relatively consistent with its initial selection as an *ADORA2A*-proximal enhancer candidate (**Figure S4B**). The subclass specific enhancers AiE0779m_3xC2 and AiE0452h_3xC2 had greater than 90% specificity for their respective cell types (90.4% STR D1 Gaba and 92% STR D2 Gaba, respectively, FIG). We observed a dynamic range in number of cells expressing enhancer-driven transcripts, with the weakest enhancer-barcode detected in 250 cells (AiE0526h) to the strongest in 2,067 cells (AiE0784m) (**Figure S4B**), suggesting large differences in completeness of striatal MSN labeling in the dorsal

striatum region between enhancers. We also counted the number of barcoded transcripts per cell as a measure of enhancer strength (**Figure S4C**). Interestingly, the full length AiE0441h expressed in a similar number of cells compared to the optimized version AiE0441h_3xC2 (1,515 cells vs. 1,718 cells, respectively), but had 2x fewer transcripts detected (median UMI = 7 vs. median UMI = 14, respectively), suggesting enhancer core concatenation improved enhancer strength without changing striatum coverage. The two strongest enhancers, AiE0784m and AiE0441h_3xC2, exhibited both broad coverage as well as higher transcript expression in the dorsal striatum (median UMI = 12 and 14, respectively).

Native SYFP2 fluorescence in sagittal sections following individual retro-orbital (RO) injection of the pan-MSN enhancer AAV vectors (**Figure S4D-E**) provided additional independent corroboration of the *in vivo* multiplex results. Similar to the multiplex cell numbers per enhancer recovered, we also observed a dynamic range in native SYFP2 fluorescence intensity. The four enhancers with the brightest SYFP2 signal (AiE0441h_3xC2, AiE0784m, AiE0450h, and AiE0367h_3xC2) matched the enhancers with the highest median transcripts in the multiplex test. AiE0526h, AiE0351h, and AiE0367h had the lowest expression across these two independent techniques.

Multimodal molecular validation confirms striatal enhancer AAV cell type specificity

We next sought to quantitatively measure enhancer specificity in the dorsal striatum by employing a combination of immunohistochemistry (IHC), single cell RNA sequencing (scRNA-seq), and RNAscope (**Figure 3A**). Using IHC for protein detection, we analyzed native enhancer-driven SYFP2 fluorescence for 15 enhancers together with striatal cell type marker antibodies (anti-Chat for cholinergic interneurons, anti-Pvalb for Pvalb-Pthlh interneurons, and anti-nNos for Sst-Chodl interneurons[15,34]). Enhancers specific for striatal D1 and D2 MSN subclasses were analyzed using SYFP2 fluorescence following RO virus injection into Drd1a-tdTomato transgenic mice and confocal imaging. To resolve the identity of enhancer AAV labeled striatal cell types, single cell RNA sequencing was performed on 24 enhancers using Smart-seq v4 (SSv4) on isolated SYFP2$^+$ whole cells dissociated from the dorsal striatum region. We collected and sequenced on average 53 cells per experiment (one enhancer AAV vector RO injected into one mouse; average cells +/-SD = 53 +/- 17.01) for a total of 1,267 cells. Cell subclasses were defined by mapping the cells to the mouse whole brain taxonomy using the MapMyCells hierarchical mapping (https://portal.brain-map.org/[30]). (**Figure 3B**). Lastly, we performed multiplex fluorescent in situ hybridization (mFISH) using RNAscope for 22 enhancer AAVs using probes against SYFP2 and well-known striatal cell type marker genes *Ppp1r1b* (pan-MSNs), *Drd1* (D1 MSNs), *Drd2* (D2 MSNs), and *Chat* (cholinergic interneurons) (**Figure S5**).

We compared the specificity of each enhancer AAV calculated from all three modalities (**Figure 3C**). In general, all enhancers exhibited high specificity for their designated cell subclass (overall specificity across techniques +/- SD = 88.3% +/- 13.1%) and all techniques were mostly in agreement (IHC average specificity +/- SD =85.57% +/- 13.86%, SSv4 average specificity +/- SD=90.08% +/- 13.21%, RNAscope average specificity +/- SD =88.13% +/- 12.02%). For our exemplary D1 and D2 MSN enhancers we obtained specificity values across modalities that were in close agreement in support of very high specificity at the subclass level. For D1 MSN enhancer AiE0779m_3xC2 the specificity was calculated as 99% by IHC (SYFP2$^+$tdTomato$^+$/SYFP2$^+$) and 100% by scRNA-seq and taxonomy mapping. For D2 MSN enhancer AiE0452h the specificity was 96% by IHC (SYFP2$^+$tdTomato$^-$/SYFP2$^+$) and 97% by scRNA-seq and mapping. In both cases the specificity was slightly lower by mFISH/RNAscope (88% and 83% subclass specificity, respectively), although still in close agreement. Slightly lower values could be due to high noise in mFISH cell segmentation and image analysis or the preferential collection of bright cells by FACS.

.

A relatively larger disparity in specificity measurements between techniques was found for enhancers labeling the Pvalb-Pthlh interneuron subclass, where specificity values determined by SSv4 was considerably higher than by IHC (SSv4 average +/- SD =92.33% +/- 4.41% vs. IHC average +/- SD =65.83% +/- 9.7%). This aligns with recent evidence indicating that *Pvalb* expression is found in many but not all interneurons belonging to this striatal neuron subclass[28]. Accordingly, we report that the SSv4 approach is better suited for determining the specificity of striatal Pvalb-Pthlh subclass enhancers, since this technique utilizes the collective transcriptome for mapping as opposed to relying on a single marker gene. With this in mind, we validated four different striatal Pvalb-Pthlh interneuron enhancers with specificity ranging from 87-97% at the subclass level by SSv4. We also validated five novel striatal Sst-Chodl interneuron enhancers with specificity ranging from 87-100% at the subclass level and with close agreement between IHC and SSv4 (**Figure 3C**), thus mFISH analysis was not deemed necessary.

We cloned a previously identified 894 bp human *Chat* promoter fragment (hChATp) into our AAV vector design for comparison to our enhancers for labeling striatal cholinergic interneurons. This human *Chat* promoter fragment was previously used in canine adenoviral (CAV) and AAV vectors to achieve enriched labeling of cholinergic neurons following stereotaxic injection into the mouse, rat and macaque striatum with specificity ranging from 64-86% specificity for $ChAT^+$ neurons[46,47]. Here, we tested the hChATp for brain wide specificity of labeling in mouse following RO delivery in our platform. Four of our novel cholinergic enhancers achieved higher specificity of labeling in the dorsal striatum by the three quantification methods (**Figure 3C**) and with lower off-target expression in cortex, substantia innominata, and hindbrain regions, as illustrated by ChAT co-staining images for AiE0743m_3xC2 relative to hChATp (**Figure 3D-E**). Our best-in-class striatal cholinergic enhancer AiE0873m_3xC2 achieved a consensus of >90% specificity at the subclass level by all three quantification methods (IHC, SSv4, and mFISH), as compared to a highest value of 62% specificity for hChATp by IHC.

In addition to quantifying specificity of labeling we also measured signal intensity in RNAscope experiments to compare SYFP2 reporter expression levels between the full length AiE0779m enhancer with the optimized versions, AiE0779m_3xC2 and AiE0779m_6xC2, extending our previously established enhancer core concatenation approach[21,22]. We found the number of concatenated enhancer cores was positively correlated with both enhancer strength and completeness of labeling (**Figure 3F-G**).

Comparison of striatal enhancer performance by different routes of virus administration

It was previously reported that stereotaxic injection of neocortical cell type enhancer AAVs led to lower cell type specificity values as compared to RO injection of the same vectors[21]. Given the relative dearth of evidence along these lines, it is important to evaluate enhancer specificity for different routes of AAV administration and to document the optimal dose ranges associated with each route (**Figure 4A**). We tested a subset of exemplary striatal cell type enhancers driving SYFP2 reporter transgene by three different routes of administration (RO, ICV, and stereotaxic injection) and compared the specificity of labeling (**Figure 4B-E**). For D1 MSN enhancers (AiE0779m and AiE0780m) and D2 MSN enhancer (AiE0452h) we qualitatively evaluated specificity by analysis of direct versus indirect pathway axon projection targets (**Figure 4F**). D1 MSN enhancer AiE0779m drove on-target SYFP2 expression by RO and ICV routes but exhibited an apparent loss of specificity by stereotaxic injection based on dense axon terminal labeling observed in GPe in addition to GPi and SNr (**Figure 4B**), despite multiple rounds of iterative adjustment to AAV dosage (data not shown). Importantly, D1 MSNs are known to have relatively sparse axon collaterals terminating in GPe in addition to GPi and SNr[48,49], however, the observed pattern and density of GPe axon terminal labeling was more consistent with overt loss of specificity. In contrast, clear on-target labeling of direct pathway D1 MSNs was observed for AiE0780m by all routes of AAV delivery (**Figure 4C**). Similarly, exemplary D2 MSN enhancer AiE0452m yielded

strong on target SYFP2 expression in direct pathway D2 MSNs with all routes of administration (**Figure 4D**).

For striatal interneuron subclass enhancers (cholinergic: AiE0873m_3xC2 and AiE0743m_3xC2; Pvalb-Pthlh: AiE0140h_3xC2; Sst-Chodl: AiE0769m and AiE0682h) we performed immunostaining with cell type marker antibodies (ChAT, Pvalb, and nNos, respectively) and quantified specificity of labeling in the target subclass in the dorsal striatum region by each route of virus administration (**Figure 4G**). In all cases the specificity of labeling was highest with RO injection (range of 80%-98% specificity) and lowest with stereotaxic injection (range of 26%-88% specificity). The ICV injection route produced intermediate specificity values (range 63%-91%). The lower specificity observed with stereotaxic injection versus RO injection for this set of striatal interneuron enhancer AAV vectors may indicate that further optimization of the injection dose is necessary, although specificity was likely at or near optimal for Sst-Chodl enhancer AiE0769m at 88% vs. 98% and cholinergic enhancer AiE0743m_3xC2 at 79% vs. 97% for stereotaxic vs. RO, respectively. For the second cholinergic enhancer AiE0873m_3xC2, the specificity of labeling by RO (94%) and ICV (88%) routes was exceptionally high but fell precipitously with stereotaxic injection route (26%). Examination of the dorsal striatum high magnification images revealed many smaller putative MSNs detected by antibody amplification of the SYFP2 signal, in addition to the large $ChAT^+$ cholinergic neurons (**Figure 4H**).

Versatility of striatal enhancers for expression of diverse transgene cargos

Similar to route of administration, the packaged transgene cargo could also impact vector expression level or specificity[50]. To directly address this possibility, we swapped out SYFP2 for several commonly used functional cargos including channelrhodopsin variant CoChR-EGFP and the calcium indicator jGCaMP8m for direct expression under the control of our best-in-class D1 and D2 MSN enhancers (**Figure 4I-J**). The packaged AAVs were administered into the dorsal striatum by stereotaxic injection (**Figure 4I**), a route frequently used for neural circuit dissection, and qualitatively checked for specificity and expression by native fluorescence and evaluation of axon projection targets of the direct versus indirect pathway. Viral dose was titrated to determine the optimal dose for balancing intended cell type specificity with robust transgene expression level. In contrast to the optimal stereotaxic injection dose of 1E+9vg for D2 MSN expression of SYFP2 under the AiE0452h enhancer (**Figure 4D**), we found that the optimal dose for expression of CoChR-EGFP was two times higher at 2E+9vg and five times higher at 5E+9vg for jGCaMP8s, indicating that these transgenes are relatively more difficult to express in striatal MSNs than SYFP2. Nonetheless, the specificity of labeling was well-maintained, as judged by selective axon terminal labeling in the GPe with no axon terminal labeling seen in GPi or SNr regions in both cases (**Figure 4J**).

Another use case for our striatal enhancer AAVs is cell type-specific conditional gene deletion using Cre/loxP technology. Typically, this is achieved by crossing transgenic mouse lines with loxP flanked (i.e., 'floxed') exons or gene loci to transgenic Cre driver lines, where Cre recombinase is expressed under the control of endogenous cell type specific regulatory elements[51]. Similarly, Cre-dependent expression can be achieved by crossing cell type-specific Cre driver lines with Cre-dependent reporter lines (**Figure 5A**), such as Ai14 Cre-dependent tdTomato reporter line[52]. While there are several options for transgenic mouse lines driving Cre recombinase in striatal D1 and D2 MSNs[53,54], many have extensive extra-striatal labeling (either consistent with endogenous gene expression patterns or ectopic in nature[11]) making them unsuitable for striatum-specific perturbations in disease modeling.

Two of the most specific and widely used mouse Cre driver lines are the EY217 (D1 MSN) and ER44 (D2 MSN) GENSAT BAC transgenic mice[11]. We compared EY217 and ER44 mouse line brain expression data from the GENSAT website (www.gensat.org) with two of our best-in-class MSN enhancers, AiE0779m_3xC2 (D1 MSN) and AiE0452h (D2 MSN), driving attenuated iCre(R297T), a

point mutant iCre variant that was successful at improving the fidelity of cell type specific enhancer recombination mitigating extra-striatal labeling[25,50]. The enhancer AAVs were delivered by RO injection into Ai14 Cre-dependent tdTomato reporter mice (**Figure 5B**). We observed several improvements in the enhancer AAV strategy compared to the GENSAT Cre lines. First, the D1 Cre BAC Tg mouse line EY217 exhibits expression in granule cells of the islands of Calleja in the olfactory tubercle (OT) and in layer 6 of the neocortex (**Figure 5C-D**), whereas far less labeling was seen in these regions and cell types with D1 MSN enhancer Cre driven recombination (**Figure 5E-F**). Second, in the case of D2 Cre BAC Tg mouse line ER44, there is expression of Cre recombinase in both striatal D2 MSNs and in midbrain dopamine neurons known to express the D2 receptor and that send dense axon projections to the striatum (**Figure 5G-H**). In contrast, the D2 enhancer driven Cre recombination was more striatum-restricted in D2 MSNs with no expression observed in midbrain dopamine neurons (**Figure 5I-J**). Thus, our best-in-class D1 and D2 MSN Cre AAV vectors compare favorably to widely used D1 and D2 Cre BAC transgenic mouse lines.

Cre recombination can be very sensitive as it exhibits a fourth order cooperativity for recombining loxP sites. This could be challenging to titrate under certain experimental contexts such as stereotaxic injection where the effective multiplicity of AAV infection is much higher compared to RO injection. We selected pan-MSN enhancer AiE0441h_3xC2, D1 MSN enhancer AiE0780m, and D2 enhancer AiE0452h to pair with iCre(R297T) in AAV vectors for testing cell type specific Cre recombination by stereotaxic injection into the dorsal striatum versus RO injection in adult Ai14 mice (**Figure 5K-R**). We titrated the optimal dose for stereotaxic injection experiments and achieved highly specific Cre recombination in MSNs, D1 MSNs, and D2 MSNs. The specificity of labeling was qualitatively comparable between stereotaxic injection and RO injection experiments at the respective optimal doses.

Enhancer driven ChR2 expression is sufficient for robust *in vivo* optogenetic perturbation of behavior

We next sought to establish whether enhancer driven transgene expression is sufficient to perturb striatal neuron function *in vivo*. We designed a vector AiP13278 for expression of ChR2(CRC)-EYFP in direct pathway D1-MSNs driven by enhancer AiE0779m_3xC2 and delivered the virus by ICV injection in P2 mouse pups (**Figure 6A**). The CRC variant includes mutations L132C/H134R/T159C and was designed to confer strong blue light evoked currents as described previously[55]. As a control for virus injection and fluorescent protein expression alone we injected additional mice with enhancer AAV for expression of SYFP2 in D1-MSNs using the same enhancer. Optic fibers for blue light delivery were implanted over the dorsal striatum (**Figure 6B**), and animals were used for behavioral analysis at 3-6 months old. *In vivo* optogenetic stimulation robustly induced locomotion and overt contralateral rotations in D1-ChR2 mice (n=8 mice), whereas no effect was observed with blue light stimulus in D1-SYFP2 animals (n=9 mice; **Figure 6C-I**). The blue light-induced contralateral rotations were robust across repeated trials for each session and across the entire cohort of D1-ChR2 mice. Thus, enhancer driven ChR2 in D1 MSNs of the dorsal striatum was sufficient for optogenetic control of mouse motor behavior.

Multiplex viral labeling enables targeted recordings from three distinct striatal interneuron subclasses in wild-type mice

Simultaneous viral genetic labeling and imaging of discrete striatal neuron populations using contrasting fluorophores would be highly advantageous for assaying cellular features in genetic disease models, gene deletion studies, or other paradigms where complex transgenic animal crosses are time and cost prohibitive. To demonstrate such feasibility, we performed multiplex injections of striatal cell type enhancer AAVs driving contrasting fluorophores in adult mice (**Figure 7A**). We first combined RO

injection of best-in-class D1 MSN, D2 MSN, and cholinergic enhancer AAV vectors for expression of SYFP2, monomeric teal fluorescent protein-1 (mTFP1), and tdTomato respectively. We observed mutually exclusive labeling of the direct versus indirect striatal projection pathways of the basal ganglia circuit together with the less abundant large cholinergic interneurons (**Figure 7B**). We did not observe enhancer crosstalk for this combination of striatal cell type enhancers. We also tested RO injection with enhancer AAVs for labeling pan-MSNs (AiE0447h driving SYFP2) and oligodendrocytes (AiE0410m driving mTFP1) and observed mutually exclusive labeling (**Figure S6**).

Next, we performed a different triple RO injection combination to mark each of three major interneuron subclasses: Pvalb-Pthlh in mTFP1, Sst-Chodl in SYFP2, and cholinergic in tdTomato. Using the combination of AiE0140h_3xC2 (Pvalb-Pthlh), AiE0682h (Sst-Chodl), and AiE0743m_3xC2 (cholinergic) enhancers we uncovered surprising evidence of enhancer crosstalk in the neocortex. Specifically, the AiE0743m_3xC2 cholinergic enhancer unexpectedly drove tdTomato expression in the same population of neurons marked by AiE0140h_3xC2 in the mTFP1 channel (**Figure 7C**). Notably, this pattern of widespread cortical tdTomato expression was not observed with AiE0743m_3xC2 enhancer AAV RO injection alone (**Figure S2**). Interestingly, the fluorescent protein expression patterns in the dorsal striatum region after the triple RO injection exhibited near mutual exclusivity, whereas the cortical region showed evidence of significant enhancer crosstalk (**Figure 7D-E**). To further explore this triple labeling paradigm for striatal interneuron types, we tested different combinations of novel enhancers for comparison to the preceding results. Using the combination of AiE0140h_3xC2 (Pvalb-Pthlh), AiE0743m_3xC2 (cholinergic), and alternate enhancer AiE1426m (Sst-Chodl), we no longer observed enhancer crosstalk in the brain. We instead observed exemplary mutually exclusive three-color labeling in the three distinct populations of striatal interneurons (**Figure S6**).

We next sought to show functional analysis of cellular properties by targeted patch clamp recordings (**Figure 7F-J**). We targeted the three distinct striatal interneuron types for recordings based on their respective cytosolic fluorescent protein labels and their hallmark somatodendritic morphologies (**Figure 2G**). The tdTomato$^+$ cholinergic interneurons and SYFP2$^+$ Sst-Chodl interneurons both exhibited spontaneous action potential firing, as expected from prior reports of patch clamp recordings in rodent striatum brain slices[56]. Conversely, the mTFP1$^+$ Pvalb-Pthlh interneurons had a relatively hyperpolarized resting membrane potential, low input resistance, and showed the expected fast-spiking phenotype upon suprathreshold 1s current injection steps (**Figure 7G**). FI (frequency/current) curves were measured from each recorded neuron and used to extract various intrinsic electrophysiological features for comparison. We constructed 3D plots using the most discriminatory sets of electrophysiological features (i.e., FI slope, resting membrane potential, and AP half width, or alternately, FI slope, upstroke downstroke ratio, and input resistance) and observed clear separation of the three distinct interneuron populations into three different spatial domains, consistent with their known signature electrophysiological properties in rodents[5,6] and confirming the high specificity of viral labeling in the triple RO multiplex experiment (**Figure 7I-J**). This experiment demonstrates that multiple distinct striatal interneuron types can be simultaneously labeled in adult C57Bl6/J mice for detailed analysis of intrinsic properties by patch clamp recording in acute brain slices. It is expected this approach can be applied to study cell type specific synaptic connectivity and neuromodulation in the striatum as well.

Cross-species conservation of striatal enhancer activity

Although our enhancer AAV screening pipeline was developed for the mouse brain, we note that the validated striatal cell type enhancers were derived from both mouse and human genomic sequence. Additionally, the ability to target specific cell types of the striatum has clear therapeutic potential in humans, but this depends significantly on whether their specificity is conserved across species. We thus investigated both the evolutionary conservation of chromatin accessibility at orthologous enhancer

loci in multiple species, as well as an assessment of the conservation of enhancer activity and cell type specificity in the rat and macaque brain.

To explore the evolutionary conservation of striatum-enriched chromatin accessibility at enhancer genomic loci selected as viral tools, we compared previously published bulk ATAC-seq on striatal and cortical tissues from human, mouse, and rat. Five enhancers derived from either mouse or human genomic sequences were chosen based on their high specificity of labeling in mouse striatum: three pan-MSN enhancers (AiE0441h, AiE0447h, and AiE0367h_C2), one D1 MSN enhancer (AiE0779m), and one D2 MSN enhancer (AiE0452h). Our analysis revealed that in all but one case, the ortholog of AiE0441h in rat, these enhancers exhibited enriched open chromatin activity in striatum compared to cortex across species (**Figure 8A**). This conserved pattern of striatal-enriched chromatin accessibility highlights the evolutionary conservation of regulatory elements associated with these enhancers.

We next evaluated whether these striatal-specific enhancers would show conserved activity in the rat brain *in vivo*. We injected this set of enhancer AAV vectors into P1 rat pups by ICV route and assessed the SYFP2 expression pattern in brain at P19. We found that the brain expression patterns matched the expected pan-MSN, D1 MSN, or D2 MSN activity and were clearly conserved between rat and mouse in all cases (**Figure 8B**). Notably, even in the example where the native rat ortholog of human genomic enhancer AiE0441h showed no chromatin accessibility in the striatum, this enhancer still drove pan-MSN specific reporter expression in the rat brain. We also tested the optimized enhancer AiE0441h_3xC2 and observed stronger SYFP2 expression with more complete MSN coverage throughout the striatum compared to the original full-length enhancer AiE0441h, supporting that enhancer core concatenation is a generalizable strategy for improving enhancer strength while retaining specificity in multiple mammalian species.

Finally, we performed *in vivo* injection of exemplary D1 MSN enhancer AiE0780m driving SYFP2 (vector AiP12610) into Macaque caudate and putamen to evaluate enhancer activity in the non-human primate brain (**Figure 8C-H**). We recovered the injection sites and found dense MSN labeling in the middle of the caudate and putamen regions in anterior striatum. Analysis of serial coronal sections through the macaque brain revealed selective SYFP2^{+} axon terminal labeling in the GPi and SNr, with no SYFP2^{+} axon terminal labeling observed in GPe. Lastly, we performed mFISH analysis using RNA-scope to confirm that 95% of SYFP2^{+} cell bodies in the putamen injection site and 97% in the caudate injection site were both DRD1^{+} and PPP1R1B+ (**Figure 8D**), consistent with highly specific D1 MSN labeling and strong conservation of AiE0780m enhancer activity from rodent to primate. Together, these findings underscore the robustness of these enhancers as tools for striatal cell type-specific targeting from rodent to primate brain.

Discussion

We provide a deeply validated toolbox of enhancer AAV vectors for accessing, monitoring, and perturbing major striatal neuron subclasses *in vivo*. These viral vectors are shown to achieve high specificity of labeling in the striatum following systemic (RO) delivery in mice using multiple independent approaches for molecular validation. We report best-in-class enhancer AAV vectors for pan-MSN class as well as five major striatal neuron subclasses, each with at least one or more exemplary enhancer achieving ≥90% specificity of SYFP2 reporter expression following RO injection in mice. Additionally, we compared specificity of labeling by three different routes of administration in mice (RO, ICV, and stereotaxic injection) and report optimal dose ranges for each route as a helpful guide to future users. This work nicely complements two companion studies comparing how different routes of administration influence enhancer specificity and expression level for predominantly cortical cell type targeting enhancer AAV vectors[26,45]. Continued rigorous analysis and standardized testing along these

lines will help ensure high reliability and reproducibility of labeling with the rapidly growing toolbox of cell type targeting enhancer AAV vectors for brain research.

Importantly, enhancer AAV vectors confer several unique advantages over existing transgenic mouse or rat lines in use to target striatal neuron populations. First, the enhancer AAV vectors can be rapidly modified in a matter of days to insert alternate transgene cargos, as we have demonstrated using contrasting fluorescent proteins (e.g., SYFP2, mTFP1, and tdTomato), Cre recombinase, channel rhodopsin variants (ChR2 and CoChR[57]), and genetically encoded calcium indicators (jGCaMP8 variants[58]). We demonstrated that exemplary enhancers like our optimized D1 MSN enhancer AAV vector delivered by ICV route was sufficient to drive meaningful levels of transgenes such as ChR2 to confer robust optogenetic control of motor behavior in awake-behaving mice. Second, the enhancer AAV vectors can be injected into any genotype of mice (e.g., wild type or mutant strains such as disease models) at any age without the need for complicated and expensive breeding paradigms or complex genotyping requirements. This approach can save costs and improve efficiency by shortening the time for experiments. Third, the enhancer AAV vectors can readily be packaged with different AAV capsid variants such as AAV-retro[59,60] to impart new functionality and extend their utility, in this case for axon projection mapping and intersectional circuit tracing. Most importantly, these enhancer AAV vectors can be applied to target and perturb genetically defined homologous cell types across diverse mammalian species beyond the mouse model, which addresses a critical unmet need for advancing studies of brain evolution, comparative cellular neurobiology, and development of cell type-specific therapies for treating human brain disorders.

We focused extensively on developing exemplary enhancers for direct (D1) and indirect (D2) pathway MSNs, as these neuron types have been the topic of intensive investigation in the context of basal ganglia circuit connectivity and neurophysiology[49,61,62], action selection and movement disorders[9,40,63–66], neuromodulation and drugs of abuse[67–70] for many decades. Progress in dissociating the roles of the direct versus indirect pathway striatal MSNs has been greatly accelerated by the development and broad distribution of BAC transgenic mouse lines for expression of EGFP or Cre recombinase[9–11]. We identified and validated two distinct enhancers, AiE0779m and AiE0780m, for targeting the D1 MSN subclass. These enhancers were discovered proximal to known direct pathway MSN marker genes *Slc35d3* and *Pdyn*, respectively. Core bashing and concatenation was successful for increasing strength while preserving specificity for AiE0779m but not for AiE0780m (data not shown). As such, AiE0779m_3xC2 was initially pursued as the best-in-class D1 MSN enhancer. However, in comparing different routes of administration we found that AAV vectors containing AiE0779m or AiE0779m_3xC2 (regardless of transgene cargo) exhibited loss of specificity following stereotaxic injection in the dorsal striatum, and this loss of specificity could not be circumvented by a simple titration of viral dose. In contrast, AAV vectors with AiE0780m, despite driving weak SYFP2 expression by RO injection route, were able to achieve highly specific and robust D1 MSN expression following stereotaxic injections. This important finding illustrates that some enhancers will be better suited to certain experimental applications more so than others, as opposed to the concept of a single best-in-class enhancer for all applications, and this is a major driver of why we pursued and validated multiple enhancers for each striatal neuron subclass. On a related note, we would like to emphasize that enhancers showing weak but specific activity by RO delivery should not be overlooked for applications requiring direct stereotaxic injection into brain parenchyma. Such enhancers may prove to be exceptional in that context with adequate empirical testing.

Our exemplary D2 MSN enhancer AiE0452h exhibited high specificity of labeling with direct expression of fluorescent protein by all three routes of AAV administration. AiE0452h was also ideal for driving the attenuated iCre mutant (R297T) for D2 MSN specific recombination in multiple different Cre-dependent reporter mouse lines following RO or stereotaxic injection. In contrast, we observed that RO injection of enhancer AAV vectors nearly always resulted in suboptimal direct expression of GCaMP and ChR2

variants (often with little or no detected expression of the fused fluorescent reporter gene based on native fluorescence), and this was true even for exemplary enhancers such as AiE0452h. We propose this could be readily improved by development of more efficient capsids for BBB crossing in mouse brain or stronger minimal promoters compared to the ones we have employed. Until then, either ICV or stereotaxic injection remain the preferred route for direct enhancer driven expression of transgene cargos for optical monitoring and manipulation of neuronal activity. We also created AiE0452h_3xC2 with stronger expression in D2 MSNs of the striatum but observed unexpected off-target activity in L5 extratelencephalic-projecting neurons of the neocortex. Nonetheless, this boost in striatal D2 MSN expression strength could be leveraged for improved GCaMP or ChR2 expression by direct stereotaxic delivery to the dorsal striatum without spread to the cortex region. The depth of our enhancer AAV toolbox offers many different solutions to achieve the desired transgene expression in specific striatal neuron populations using either direct or Cre-mediated approaches. Further *in vivo* analysis will be required to fully delineate the relative strengths and weaknesses of these different enhancer AAV expression strategies with different functional transgene cargos and to evaluate any differences in tolerability of expression (short and long term) across the different striatal neuron subclasses.

Our multiplexing experiments were designed with the fact in mind that many modern neuroscience research labs commonly rely on complex transgenic mouse line crosses (either alone or in combination with viral vectors[71,72]) to generate large cohorts of experimental animals for behavioral, electrophysiological, neurochemical, and anatomical studies to uncover fundamental properties of brain cell types and circuits. The cost can be exorbitant and prohibitive for all but the most well-funded laboratories. For many neuroscience researchers these collections of enhancer AAV vectors can be a welcome alternative and should enable previously challenging or infeasible experimental approaches. For example, we have shown concomitant labeling of direct versus indirect pathway MSNs together with striatal cholinergic neurons with contrasting fluorescent proteins, as well as triple labeling of striatal Pvalb-Pthlh, Sst-Chodl, and cholinergic interneuron subclasses in wild type C57 mice following a simple RO injection procedure. These validated cell type targeting combinations alone could support wide ranging experiments into striatal cell type and circuit function without the need to invoke any transgenic rodent lines. We have shown direct applicability of striatal cell type targeting enhancer AAVs for use in rats, where availability of transgenic driver and reporter lines is much more limited than for mouse (but see also[73,74]). We envision this approach will also greatly benefit those characterizing the cellular effects of gene knockout mutations or utilizing genetic mouse models of basal ganglia disorders (e.g., mouse models of Parkinson's disease, Huntington's disease, obsessive-compulsive disorder, and autism spectrum disorders), as well as efforts to use cell type specific AAV vectors for Cre recombination in floxed mouse lines with temporal and spatial precision[75] and without the risk of confounds like germline recombination[76] or to achieve cell type specific AAV CRISPR/Cas9[77] in building on the current capabilities[78,79]. We demonstrated targeted patch clamp recording of three major striatal interneuron subclasses in acute brain slices following triple RO injection in adult mice for analysis of signature neuron intrinsic properties, an approach which can readily be applied in mouse disease models to greatly accelerate efficiency and speed of experimental progress. Direct enhancer driven ChR2 expression can be used for optotagging *in vivo* and reliable identification of striatal neuron types for extracellular recording during behavior as shown in mice[80–82], but also now extensible to diverse mammalian species.

The enhancer AAV toolbox is not without limitations. Enhancer transcriptional crosstalk has recently been recognized as a major limitation for multiplex screening or targeting using cell type specific enhancer AAV[83], and as such should be carefully considered in developing experimental designs. Enhancer crosstalk is a process whereby two or more distinct enhancer AAV genomes occur within the same cell and can interact (likely though concatenation of DNA) to cross-activate spurious transgene expression leading to confounding results, namely loss of intended cell type specificity. While we successfully achieved cases of enhancer multiplexing without overt crosstalk in this study, we also

identified specific combinations that did exhibit crosstalk. Our work adds to the intrigue around cell type enhancer crosstalk mechanisms by revealing two important and previously unknown principles. First, we observed that crosstalk between distinct cell type specific enhancers can occur in a brain region specific manner, which we speculate may relate to the effective strength of enhancer driven transgene expression across brain regions. In support of this view, AiE0140_3xC2 drives very strong expression in cortex but weaker expression in striatum Pvalb-Pthlh interneuron subclass. Accordingly, crosstalk was observed in combination with AiE0743m_3xC2 in the cortex but not striatum. Second, crosstalk between cell type enhancer AAV vectors can be mitigated (or modulated) by judicious introduction of select cell type enhancers, which must be determined through empirical testing. While the underlying detailed molecular mechanisms behind these observations remain elusive, these findings provide important context and clues about cell type enhancer AAV multiplexing in the brain. Until these mechanisms are better understood, it is necessary to test and carefully evaluate enhancer crosstalk in any experimental paradigm requiring multiplexing. In the short term, one at a time and low multiplexing of enhancer AAVs will be the most reliable option with the least potential confounds.

In summary, we present a comprehensive enhancer AAV toolbox that enables precise targeting and manipulation of distinct neuronal subclasses in the striatum. Our collection provides a valuable new resource for the neuroscience community that will facilitate in-depth studies of striatal cell type and circuit function across diverse mammalian species including non-human primates. Given that AAV vectors have been shown to be safe and effective in humans, our collection of striatal cell type specific enhancer AAV vectors may also hold great promise for targeted AAV gene replacement therapies or circuit therapies to treat various disorders of the basal ganglia.

Methods

Animals

All procedures involving mice and rats were approved by the IACUC at the Allen Institute for Brain Science (protocols 2004, 2105, 2301, 2306, 2406, and 2010). Mouse tissue was obtained from 4 to 12-week-old male and female pure C57Bl6/J or Drd1a-tdTomato line 6 hemizygous mice[13]. Animals were provided food and water ad libitum and were maintained on a regular 12-h day/night cycle with no more than five adult animals per cage. Timed-pregnant adult female Sprague-Dawley rats were ordered from Charles River Laboratories and acclimated several days after shipment prior to birth of the pups. Rat pups were tattooed at 1-day postnatal (P1) for identification purposes and used the same day for unilateral intracerebroventricular (ICV) injection of AAV vectors. Rat pups were placed back into the home cage with littermates and the dam until they were euthanized at P19 for brain harvest and transgene expression analysis.

Enhancer selection and genomics analyses

Marker genes for major mouse striatal neuron classes and subclasses were determined from published studies[42,43], databases of transgenic mouse lines, e.g., GENSAT (https://www.gensat.org/[9]), as well as using the Allen Brain Atlas and AGEA tool (https://mouse.brain-map.org/agea[84]) and DropVis mouse scRNA-seq data browser (http://dropviz.org/[29]). To identify short genomic DNA fragments (~250bp-750bp) representing putative cell type specific striatal enhancers, we analyzed publicly available ATAC-seq datasets including Roussos lab Brain Open Chromatin Atlas (BOCA[35]) human postmortem bulk ATAC-seq dataset (https://labs.icahn.mssm.edu/roussos-lab/boca/), as well as the *Cis*-element Atlas (CATlas[36]) mouse snATAC-seq dataset (http://catlas.org/mousebrain/#!/). We searched for differentially accessible open chromatin peaks within ~500kb of the top marker gene loci such as *Drd1*/*DRD1*, *Drd2*/*DRD2*, *Adora2A*/*ADORA2A*, *Penk*/*PENK*, *Enk*/*ENK*, *Gpr6*/*GPR6*, etc. Enhancer candidates were prioritized based on strong accessibility in striatal brain regions and/or cell types in comparison to all non-striatal regions and cell types. For analysis of Roussos BOCA the putamen and nucleus accumbens were available as independent ROIs/tracks, thus enabling a search for candidate

enhancers with possible enrichment in dorsal versus ventral striatum. Bulk ATAC-seq data was deemed suitable for abundant striatal neuron populations (e.g., pan-MSN and direct versus indirect pathway projecting MSN subclasses) but presumably would not be suitable for rare cell types (e.g., various striatal interneuron subclasses). As such, CATlas mouse snATAC-seq dataset was used to search for enhancer candidates with predicted activity in both rare and abundant striatal neuron populations.

Accessibility counter screening in human whole body was performed by first downloading bigwig files from Zhang et al.[85] (http://catlas.org/humanenhancer/#!/). To assess the accessibility of each putative enhancer in human tissues we used `multiBigwigSummary` from deeptools. This tool measures for each enhancer the average number of fragments within the enhancers genomic coordinate per tissue. LiftOver coordinates in hg38 were used for all enhancers found in mouse datasets (all enhancers ending in an "m") except for AiE0769m, which does not have an orthologous enhancer identifiable by liftover in hg38.

Enhancer cloning into AAV vectors

Enhancers were cloned from human or C57Bl/6J mouse genomic DNA using enhancer-specific primers and Phusion high-fidelity polymerase (M0530S; NEB). Individual enhancers were then inserted into a recombinant single-stranded pAAV backbone that contained the beta-globin minimal promoter, fluorescent reporter gene (typically SYFP2), minimal woodchuck hepatitis posttranscriptional regulatory element (WPRE3), and bovine growth hormone polyA using standard molecular cloning as previously described[21,22]. Plasmid integrity was verified via Sanger DNA sequencing and in some cases restriction digestion with agarose gel electrophoresis to confirm intact inverted terminal repeats (ITRs). In some cases, synthetic enhancer sequences such as concatenated cores were gene synthesized and subcloned into AAV vectors using standard restriction enzyme digestion and ligation. All AAV plasmids were propagated in NEB stable *E.coli* at 30°C growth condition to prevent spurious DNA rearrangements.

AAV packaging and titer determination

Small-scale crude AAV preps were generated by triple transfecting 15 µg ITR plasmid, 15 ug AAV capsid plasmid, and 30 ug pHelper (Cell Biolabs) into one 15-cm plate of confluent HEK-293T cells using PEI Max (Polysciences Inc., catalog # 24765-1). At one day post-transfection we changed the medium to low serum (1% FBS), and after 3 days the cells and supernatant were collected, freeze-thawed 3x to release AAV particles, treated with benzonase nuclease (MilliporeSigma catalog # E8263-25KU) for 1 hr to degrade free DNA, then clarified (3000g x 10min) and concentrated to approximately 150 µL by using an Amicon Ultra-15 centrifugal filter unit (NMWL 100 kDa, Sigma #Z740210-24EA) at 5000g for 30-60 min, yielding a titer of approximately 1.0E+13 to 1.0E+14 vg/mL. For large-scale gradient preps, we transfected 10 x 15-cm plates of cells and purified by iodixanol gradient centrifugation. For measuring virus titers, we used ddPCR (Bio Rad; QX 200 Droplet Digital PCR System). We used primers against AAV2 ITR for amplification. Seven serial dilutions with the factor of 10 ranging from $2.5x10^{-2}$ to $2.5x10^{-8}$ were used for the measurement. Serial dilutions of $2.5x10^{-5}$ to $2.5x10^{-8}$ were used for fitting the dynamic linear range. Viral titer was calculated by averaging virus concentration of two dilutions within the dynamic linear range. A positive control of a known viral titer, and a negative control with no virus was also run along with all the samples.

Retro-orbital (RO), intracerebral ventricular (ICV) and stereotaxic (STX) injection delivery of AAV vectors

Adult C57Bl6/J mice were briefly anesthetized by isoflurane anesthesia and injected with crude PHP.eB[39] serotyped AAV virus at a dose range of 1E+10 to 1E+12vg into the retroorbital sinus of one eye in a maximum volume of 100µL. Virus stocks were diluted in sterile 1X phosphate buffered saline

(1XPBS) solution as needed to achieve the intended dose and volume. For initial screening with enhancer AAVs driving SYFP2, we routinely used 5E+11vg as the standardized RO dose. For ICV injections, C57BL/6J mouse pups and Sprague Dawley rat pups (P0-P2) were injected with 3E+10 to 1.5E+11vg of concentrated AAV vector into the lateral ventricle(s). In most experiments animals received unilateral ICV injection but in a subset of experiments some mice received bilateral ICV injections to evaluate and compare brain wide viral transduction and transgene expression. For mouse *in vivo* optogenetics experiments, C57Bl6/J mice received a unilateral (left or right) injection of 3E+10vg concentrated AAV vector stock by ICV into the lateral ventricle at P2. For stereotaxic injection surgery, adult mice or rats were deeply anesthetized to a surgical plane using an isoflurane vaporizer and placed into the stereotaxic injection frame. AAV virus was injected bilaterally into the dorsal striatum region (dSTR) using the following coordinates (in mm) relative to Bregma: anterior/posterior (A/P) 0.8, medial/lateral (M/L) ±1.6 to 2.0, and dorsal/ventral (D/V) 2.6 to 3.0. A total volume of 500 nL containing 1E+12 to 1E+13 vg/mL virus stock was delivered at a rate of 50 nL per pulse with a Nanoject II pressure injection system. Before incision, the animal was injected with Bupivacaine (2-6 mg/kg) and post injection, the animal was injected with ketofen (2-5 mg/kg) and Lactated Ringer's Solution; LRS (up to 1 mL) to provide analgesia. Mice that underwent STX injections were euthanized after 3-5 weeks post injection, transcardially perfused with 1XPBS followed by 4% paraformaldehyde (PFA), and the brains were dissected for further analysis.

Tissue processing for slide-based epifluorescence imaging

Mice were anaesthetized with isoflurane and perfused transcardially with 10 mL of 0.9% saline, followed by 50 mL of 4% PFA. The brain was removed, bisected along the midsagittal plane, placed in 4% PFA overnight and subsequently moved to a 30% sucrose solution until sectioning. From the left hemisphere, 30 µm sections were obtained along the entire mediolateral axis using a freezing, sliding microtome. Five sagittal ROIs, roughly 0.5, 1, 1.5, 2.3 and 3.5 mm from the midline, were collected and stained with DAPI and/or propidium iodide (PI) to label nuclei and to reveal cellular profiles, respectively. Stained tissue sections were slide mounted using Vectashield hardset mounting medium (Vector Laboratories, catalog # H-1400-10) and allowed to dry for 24 hours protected from light. Once the mounting medium hardened, the slides were scanned with Aperio VERSA Brightfield epifluorescence microscope (Leica) in the UV, green, and red channels, illuminated with a metal halide lamp. After passing QC, digitized images were analyzed by manual scoring of virus-mediated fluorescent protein expression throughout the brain with emphasis on striatal regions including caudoputamen, nucleus accumbens, and olfactory tubercle. Images were not acquired under matched conditions and have been adjusted to optimally highlight brain wide expression patterns for enhancer specificity comparison purposes.

Serial two-photon tomography (Tissuecyte)

Mice were perfused with 4% PFA. Brains were dissected and post-fixed in 4% PFA at room temperature for 3–6 h and then overnight at 4 °C. Brains were then rinsed briefly with PBS and stored in PBS with 0.01% sodium azide before proceeding to the next step. Agarose was used to embed the brain in a semisolid matrix for serial imaging. After removing residual moisture on the surface with a Kimwipe, the brain was placed in a 4.5% oxidized agarose solution made by stirring 10 mM $NaIO_4$ in agarose, transferred through phosphate buffer and embedded in a grid-lined embedding mold to standardize its placement in an aligned coordinate space. The agarose block was then left at room temperature for 20 min to allow solidification. Brain tissue was additionally supported by generating a polyacrylamide network throughout the agarose block and spanning the brain-agarose interface. The agarose block was first left at 4°C overnight in a solution of 4.5% Surecast (Acrylamide:Bis-acrylamide ratio of 29:1) with 0.5% VA-044 activator, diluted in PBS. Agarose blocks were then placed back into new embedding molds containing a small amount of acrylamide solution and the top surface covered with parafilm (to reduce exposure to oxygen). Finally, specimens are baked for 2 hours at 40°C and

then stored in PBS with 0.1% sodium azide at 4°C until ready to image. The agarose block was then mounted on a 1 × 3 glass slide using Loctite 404 glue and prepared immediately for serial imaging.

Image acquisition was accomplished through serial two-photon (STP) tomography using six TissueCyte 1000 systems (TissueVision, Cambridge, MA) coupled with Mai Tai HP DeepSee lasers (Spectra Physics, Santa Clara, CA). The mounted specimen was fixed through a magnet to the metal plate in the center of the cutting bath filled with degassed, room-temperature PBS with 0.1% sodium azide. A new blade was used for each brain on the vibratome and aligned to be parallel to the dorsoventral axis. Brains were imaged from the caudal end. We optimized the imaging conditions for both high-throughput data acquisition and detection of single axon fibers throughout the brain with high resolution and maximal sensitivity. The specimen was illuminated with 925 nm (EGFP, tdTomato, dTomato data) or 970 nm (SYFP2 data) wavelength light through a Zeiss ×20 water immersion objective (NA = 1.0), with 250 mW light power at objective. The two-photon images for red, green and blue channels were taken at 75 μm below the cutting surface. This depth was found optimal as it is deep enough to avoid any major groove on the cutting surface caused by vibratome sectioning but shallow enough to retain sufficient photons for high contrast images. In order to scan a full tissue section, individual tile images were acquired, and the entire stage was moved between each tile. After an entire section was imaged, the x and y stages moved the specimen to the vibratome, which cut a 100-μm section, and returned the specimen to the objective for imaging of the next plane. The blade vibrated at 60 Hz and the stage moved towards the blade at 0.5 mm per sec during cutting. Images from 140 sections were collected to cover the full range of mouse brain. It takes about 18.5 h to image a brain at an x,y resolution of ~0.35 μm per pixel, amounting to ~750 GB worth of images per brain. Upon completion of imaging, sections were retrieved from the cutting bath and stored in PBS with 0.1% sodium azide at 4°C.

Barcoded enhancer AAV multiplex assay

Cloning and synthesis of barcoded enhancer AAVs

The 8bp barcode strategy was derived from Guo et al.[86] with all fourteen barcodes used in this study designed to have a Hamming Distance >2. Barcodes were ordered as single-stranded forward and reverse compliment oligonucleotides from Integrated DNA Technologies (IDT) with 20bp overlapping homology regions on either side of the XhoI site into each parent vactor. Each oligonucleotide stock was resuspended in water to 100uM and then combined and diluted 1:500 with its pair. Oligo pairs were annealed by boiling at 100C for 5 minutes and slowly cooling to room temperature over 30 minutes. The annealed oligonucleotides were cloned into the parent vectors using In-Fusion HD Cloning Kit (Takara 639650) and transformed into chemically competent Stbl3 E. coli (ThermoFisher C737303). Individual colonies were selected for on 100 ug/mL carbenicillin plates. Plasmids were maxiprepped (Qiagen 12162) and sequence-verified using Azenta Sanger sequencing. Completed plasmids were individually packaged into PHP.eB capsid using the small-scale crude prep method (please reference above section: AAV packaging and titer determination).

Single cell isolation of tissue from mice injected with barcoded enhancer AAVs

Barcoded enhancer AAVs were pooled for a total of 9.8E11 vg (7E10 vg per enhancer AAV) and diluted in sterile 1xPBS for a final volume of 100uL. Pooled AAVs were injected retro-orbitally into adult mice. After 4 weeks incubation, single cells were isolated as described previously[29]. Mice were anesthetized with Avertin and perfused transcardially with ice-cold Cutting Buffer containing 110mM NaCl, 2.5mM KCl, 10mM HEPES, 7.5mM MgCl2, 25mM glucose, and 75mM sucrose. Following perfusions, brains were extracted and placed in a petri dish containing Cutting Buffer to generate 2mm coronal slices using a stainless steel brain matrix (Stoelting 51386). Slices containing dorsal striatum were then transferred to a second petri dish with Dissociation Buffer containing 82mM Na2SO4, 30mM K2SO4, 10mM HEPES, 10mM Glucose, and 5mM MgCl2 and dorsal striatum was isolated using a disposable

2mm tissue punch (VWR 95039-098). Tissue pieces were then placed immediately in 10mL conical tubes containing 5mL of room temperature Enzyme Buffer containing 3mg/mL Protease XXIII (Sigma-Aldrich P5380) and 10 units/mL of Papain (Worthington LK003150) dissolved in Dissociation Buffer. Submerged slides were immediately transferred to a 34C water bath for 1 hour. Following digestion, conical tubes were placed directly on ice and the supernatant was carefully removed and replaced with 10mL Stop Solution containing 1mg/mL Trypsin Inhibitor (Sigma-Aldrich T6522), 2mg/mL BSA (Sigma-Aldrich A2153), and 1mg/mL Ovomucoid Protease Inhibitor (Worthington LK003150) dissolved in Dissociation Buffer. Tissue chunks were triturated using fire-polished glass Pasteur pipets with successively smaller bore holes while avoiding bubbles until a homogenous solution was obtained. Triturated tissue was centrifuged at 300xg for 10min at 4C, supernatant decanted, pellet resuspended in 5mL of Stop Solution, and then centrifuged again at 300xg for 10min at 4C. Following centrifugation, the supernatant was decanted once more and the cell pellet was resuspended in 500uL-1mL of Dissociation Buffer with 0.1% BSA, 1:500 DAPI (ThermoFisher 62248), and 1:500 Vibrant DyeCycle Ruby Stain (ThermoFisher V10309). The resulting single cell suspensions were filtered using a pre-wet 70µm filter (Miltenyi Biotec 130-098-462) and incubated in the dark at 4C for 30 minutes prior to flow cytometry.

Cell suspensions were sorted for SYFP2 expression using a 130µm nozzle on a BD FACSAria III at a flow rate of <2000 cells per second on purity mode. Live cells were selected for by a DAPI-negative, Ruby-positive gate. Approximately 45,000 SYFP2^{+} and SYFP2^{-} cells were collected in chilled 5mL FACS tubes containing 300uL Dissociation Buffer with 0.1% BSA. The sorted cells were centrifuged at 300xg for 10min at 4C, supernatant decanted, and the pellet resuspended in 80-100uL of Dissociation Buffer with 0.1% BSA on ice. Cell concentrations were estimated using a disposable hemocytometer (Thomas Scientific 1190G82) and 15,336 SYFP2^{+} whole cells were immediately loaded on the 10X v3.1 chip for insertion into the 10X Genomics Chromium controller.

10X Genomics, custom AAV barcode library generation, and sequencing

For GEX library generation, the manufacturer's instructions for cell capture, barcoding, reverse transcription, cDNA amplification and library construction were followed. Libraries were sequenced on the Illumina NovaSeq 6000 with a target read depth of 125,000 reads per cell. To generate custom libraries for the AAV barcoded transcripts, 10ng of the remaining amplified cDNA from each sample was first used in a 100uL reaction containing 50uL KAPA Hifi Mastermix (Roche 7958935001), 0.5uL 100uM forward primer that binds to the WPRE3 in the AAV vector 5' AACTCATCGCCGCCTGCCTTG 3' and 0.5uL 100uM reverse primer that binds to Read 1 (part of the oligo attached to the 10X gel bead) 5' CTACACGACGCTCTTCCGATCT 3' and amplified using a thermocycler with the following conditions: 98C for 5 minutes initial denaturation, then 8x cycles of 95C for 15 seconds, 60C for 30 seconds, 72C for 20 seconds, and lastly 72C for 30 seconds. The reaction was purified using 0.7x and 0.9x SPRI beads (Beckman Coulter B23318) and then resuspended in 40uL Buffer EB (Qiagen 19086). A second reaction containing 20uL of product from the first reaction, 0.5uL of 100uM nested forward primer 5' AATGATACGGCGACCACCGAGATCTACAC**NNNNNNNNNN**ACACTCTTTCCCTACACGACGCTCTTCCGATCT 3', 0.5uL of 100uM reverse primer 5' CAAGCAGAAGACGGCATACGAGAT**NNNNNNNNNN**GTGACTGGAGTTCAGACGTGTGCTCTTCCGATCTACTGACAATTCCGTGGCTCG 3', and 50uL KAPA HiFi MasterMix was used to add sequencing adapters and indexes to the amplicons. The thermocycler conditions were kept the same as the first PCR except for the cycle number was increased to 12x. The reaction was purified using 0.7x and 0.9x SPRI beads, resuspended in 25uL Buffer EB, and checked for purity and concentration using the High

Sensitivity Kit (Agilent 067-4626) on a Bioanalyzer. Custom libraries were pooled prior to sequencing on the Illumina NextSeq 2000 with a target read depth of 40,000 reads per cell.

Sequencing, QC filtering, and enhancer specificity calculations
A custom reference was created using the 10x Genomics Cellranger mkref to add the AAV vector sequences to the mouse reference transcriptome (M21, GRCm38.p6). Fastq files were aligned to the custom reference using the 10x Genomics CellRanger pipeline (version 6.1.1) while also including a feature barcode reference with directories to the AAV barcode libraries, as instructed by 10x Genomics Feature Barcode Technology manual. The pattern used to identify the AAV barcodes was 5' (BC)CGAGAGATCTTCGAC 3'. High-quality cells were selected for using stringent QC filtering as described previously[30]. Cells with total reads that contained transcripts from >20% mitochondrial genes, <2000 genes detected, and a doublet score of >0.3 (DouletFinder algorithm from scrattch.hicat https://github.com/AllenInstitute/scrattch.hicat) were removed from the dataset resulting in 8,671 high quality cells. Filtered gene x cell count matrices were then normalized using the logCPM function (also part of the scrattch.hicat R package) and then mapped using the correlation mapping strategy from scrattch.mapping (https://github.com/AllenInstitute/scrattch.mapping) onto the 10X Whole Mouse Brain taxonomy (CCN20230722). Cells that contained <2 AAV transcript UMIs were also discarded. The resulting 6,577 cells were assigned to each enhancer by the expressed enhancer-paired barcode, with 43% (2878/6577) of the cells assigned to more than one enhancer-barcode. Enhancer specificity was determined by number of cells in each cell subclass with viral vector derived transcripts and enhancer AAV strength was determined by average transcript UMI per cell.

Immunohistochemistry
Brain slices were fixed in 4% PFA in phosphate buffered saline (PBS) at 4 °C overnight or up to 48 hours and then transferred to 1XPBS with 0.01% sodium azide as a preservative. Fixed slices were thoroughly washed with PBS to remove residual fixative, then blocked for 1 hr at room temperature in 1XPBS containing 5% normal goat serum and 0.2% Triton-X 100. After blocking, slices were incubated overnight at 4 °C in blocking buffer containing one or more of the following primary antibodies: chicken anti-GFP (Aves, 1:1000 or 1:2000), rabbit anti-red fluorescent protein (Rockland, 1:500), mouse anti-ChAT IgG2b (Atlas Labs, 1:1000), Rabbit anti-nNos (Immunostar, 1:1000), Rabbit anti-Pvalb (Swant, 1:2500). Following the overnight incubation, slices were washed for 15 min three times with 1XPBS and then incubated for 2 hr at room temperature in dye-conjugated secondary antibodies (1:1000; Invitrogen, Grand Island, NY) including BV480 (goat anti-rat)Alexa Fluor 488 (goat anti-chicken), Alexa Fluor 555 (goat anti-rabbit and goat anti-mouse), and Alexa Fluor 647 (goat anti-mouse). Slices were washed for 15 min three times with 1XPBS, followed by 5ug/mL DAPI nuclear staining for 15 min. The slices were then dried on glass microscope slides and mounted with Fluomount G (SouthernBiotech, Birmingham, AL). Slides were stored at room temperature in the dark prior to imaging. Whole slice montage images were acquired with NIS-Elements imaging software on a Nikon Eclipse Ti or Ti2 Inverted Microscope System equipped with a motorized stage and epifluorescence illumination with standard DAPI, FITC, TRITC, Cy3, and Cy5 excitation/emission filter cubes. Confocal z-stack images were acquired on an Olympus Fluoview 3000 laser scanning confocal microscope equipped with 488 nm, 543 nm, 594 nm, and 647 nm excitation laser lines.

Specificity of enhancer activity for the target striatal cell subclass or type was quantified as reporter and marker Ab double positive neuron count divided by total reporter Ab positive neuron count and multiplied by 100 to obtain a percentage. The main ROI for analysis was in the center of the dorsal striatum region. A minimum of 50 neurons were counted in each ROI. Completeness of labeling of a given target striatal cell subclass or type was quantified as reporter and marker Ab double positive

neuron count divided by total marker positive neuron count and multiplied by 100 to obtain a percentage.

RNAscope

Mouse: We performed RNA FISH using RNAscope Multiplex Fluorescent v1 and v2 kits (Advanced Cell Diagnostics) according to the manufacturer's protocols. For the v1 kit, 10µm mouse brain sections were prepared from fresh frozen brains and embedded in optimum cutting temperature compound (OCT; Tissue-Tek). For the v2 kit, 30µm sections were prepared from mice perfused with 4% PFA, the brain extracted and sunk in 30% sucrose before OCT embedding. All coronal sections for both kits were cut using a cryostat (CM3050 S) and mounted on SuperFrost slides (ThermoFisher Scientific). Slides were stored at −80 °C and used within one month. For the v2 kit, during the sample preparation and pretreatment step, we increased the slide baking time from 30 minutes in the manual to 1 hour to improve tissue adherence. When developing HRP signal, the HRP blocking step was increased from 15 minutes in the manual to 30 minutes to minimize cross amplification between the different channels/probes. The following probes were used: ChAT (ACD Cat#408731-C2) to label PAL-STR Gaba-Chol cells, Ppp1r1b (ACD Cat#405901-C2 or ACD Cat#405901-C3) to label all MSNs, Drd1 (ACD Cat#461901-C3) to label D1 MSNs, Drd2 (ACD Cat#406501-C3) to label D2 MSNs and SYFP2 mRNA (ACD Cat#590291-C1) for detecting enhancer-driven transcripts. To visualize the probes, we used the following TSA dyes and concentrations from ACD: TSA Vivid 520 (1:1500, Cat# 7534) for SYFP2, TSA Vivid 570 (1:2000, Cat#7535) for ChAT, Drd1, and Drd2, and TSA Vivid 650 (1:5000, Cat#7536) for Ppp1r1b. DAPI (Cat#323108) labelled nuclei. We imaged slides at 40X on a confocal microscope (Leica SP8). Specificity measurements for the dorsal striatum were determined using QuPath cell detection and object classifiers[87]. The DAPI nuclear signal was used to segment cells in images. We did note some bleed-through of probes between the channels (especially with the Ppp1r1b probe which had an exceptionally strong signal). To quantify real signal over background, we trained QuPath object classifiers separately for each probe using individual training images before applying to the ROI. Specificity of enhancer AAVs was calculated as follows: $SYFP2^{+}Chat^{+}$ / $SYFP2^{+}$ for cholinergic interneuron enhancers, $SYFP2^{+}Ppp1r1b^{+}$ / SYFP2+ for pan-MSN enhancers, $SYFP2^{+}Drd1^{+}$ / $SYFP2^{+}$ for D1 MSN enhancers, and $SYFP2^{+}Drd2^{+}$ / $SYFP2^{+}$ for D2 MSN enhancers.

Macaque: The RNAscope Multiplex Fluorescent v2 kit was used in tandem the RNA-Protein Co-detection Ancillary kit (ACD) with a few modifications. The tissue was cut using a freezing sliding microtome and mounted on SuperFrost slides (ThermoFisher Scientific). Slides were stored at −80 °C and used within one month. During sample preparation and pretreatment, we performed the hydrogen peroxide wash first before allowing the sections to air dry for 2 hours on the slide. The slide baking step was increased from 30 minutes to 1 hour for improved tissue adherence. We added an additional 15-minute baking step after the EtOH washes also for improved tissue adherence. Due to loss of native SYFP2 signal from the v2 kit protocol, we incorporated the RNA-Protein Co-detection kit to perform IHC to visualize the enhancer driven SYFP2 while using the probes for the marker gene mRNA. We followed the co-detection kit protocol and placed the tissue in primary antibody solution at 4C after the antigen retrieval step where it incubated overnight. The primary antibody used to visualize the SYFP2 was chicken anti GFP (1:250, Aves Lab Cat# GFP1020). The secondary antibody incubation occurs after the final HRP blocking step. The tissue is placed in secondary antibody solution for 3 hours at room temperature. The secondary antibody used was goat anti chicken Alexa Fluor 488 (1:500, Invitrogen Cat#A11039). Two probes were used: Drd1 (ACD Cat# 1075621-C2) to label D1 MSNs and Ppp1r1b (ACD Cat# 1075651-C1) to label all MSNs. To visualize the probes, we used the following TSA dyes and concentrations from ACD: TSA Vivid 570 (1:1500, Cat#7535) for Ppp1r1b and TSA Vivid 650 (1:1500, Cat#7536) for Drd1. DAPI (Cat#323108) labelled nuclei. All slides are mounted with ProLong Gold Antifade mounting media (ThermoFisher Scientific Cat#P36930) and allowed to dry overnight before imaging on a Nikon Eclipse Ti2 Inverted Microscope System equipped with a motorized stage and epifluorescence illumination with standard DAPI, FITC, TRITC, Cy3, and Cy5

excitation/emission filter cubes. To quantify specificity, images were loaded into FIJI where brightness/contrast was manually adjusted to eliminate background signal in all channels. Cells were then marked using the Cell Counter plugin based on positivity for GFP, Drd1, and Ppp1r1b. Specificity was calculated as $GFP^+Drd1^+Ppp1r1b^+$ / GFP^+.

SMART-seq v4 sample preparation and analysis (scRNA-seq)

Single cell suspensions from enhancer AAV RO injected mice were prepared for flow cytometry and single cell RNA-seq from brain tissue as previously described[88]. Briefly, for flow cytometry, we perfused mice transcardially under anesthesia with ACSF.1. We harvested the brains, embedded in 2% agarose in PBS, then sliced thick 350 micron sections using a compresstome with blockface imaging, then picked the sections containing the dorsal striatum and dissected it out. We then treated dissected tissues with 30U/mL papain (Worthington LK003176) in ACSF.1 containing 30% trehalose (ACSF.1T) in a dry oven at 35°C for 30 minutes. After papain treatment we quenched digestion with ACSF.1T containing 0.2% BSA, triturated sequentially using fire-polished glass pipettes with 600, 300, and 150 micron bores, filtered the released cell suspensions into ACSF.1T containing 1% BSA, centrifuged cells at 100g for 10 min, then resuspended cells in ACSF.1T containing 0.2% BSA and 1 µg/mL DAPI prior to flow cytometry and sorting on a FACSAria III (Becton-Dickinson). Sample preparation for SMART-Seq was performed using the SMART-Seq v4 kit (Takara Cat#634894) as described previously[88]. Single cells were sorted into 8-well strips containing SMART-Seq lysis buffer with RNase inhibitor (0.17 U/µL; Takara Cat# ST0764) and were immediately frozen on dry ice for storage at −80°C. SMART-Seq reagents were used for reverse transcription and cDNA amplification. Samples were tagmented and indexed using a NexteraXT DNA Library Preparation kit (Illumina Cat#FC-131-1096) with NexteraXT Index Kit V2 Set A (Illumina Cat#FC-131-2001) according to manufacturer's instructions except for decreases in volumes of all reagents, including cDNA, to 0.4 x recommended volume. Full documentation for the scRNA-seq procedure is available in the 'Documentation' section of the Allen Institute data portal at http://celltypes.brain-map.org/. Samples were sequenced on an Illumina HiSeq 2500 as 50 bp paired end reads. Reads were aligned to GRCm38 (genecode v23) using STAR v2.7.1 with the parameter "twopassMode," and exonic read counts were quantified using the GenomicRanges package for R as described in Tasic et al. (2018). To determine the corresponding cell type for each scRNA-seq dataset, we utilized MapMyCells hierarchical mapping from the Allen Institute http://celltypes.brain-map.org/ according to the posted instructions against the 10x Whole mouse brain taxonomy (CCN20230722). We applied quality control steps to exclude cells from the dataset if they had less than 1,000 genes detected (63 cells; 5%) and if they clearly did not map to basal ganglia cell subclasses corresponding to the dissected brain regions (98 cells; 7.7%). The remaining 1,106 high-quality cells (87.3%) were used to determine enhancer AAV labeling specificities Below is a list of taxonomy cell classes and subclasses and common names they correspond to:

Taxonomy Class	**Taxonomy Subclass** (CCN20230722)	**Common cell type name**
CNU-LGE Gaba	STR D1 Gaba STR D2 Gaba STR D1 Sema5a Gaba	D1 MSN (direct pathway MSN) D2 MSN (indirect pathway MSN) D1/D2 hybrid MSNs
CNU-MGE Gaba	PAL STR Gaba-Chol STR Prox1 Lhx6 Gaba Sst Chodl Gaba	Cholinergic interneurons Pvalb-Pthlh interneurons Sst-Chodl interneurons

Comparative ATAC-seq analyses

Previously published bulk ATAC-seq data from cortex and striatum of human (GSE96949), mouse (GSE161374), and rat (GSE159815) were obtained from NCBI's GEO Database. We combined all available replicates available in bigWig format in human (n = 9 primary motor cortex; n = 10 putamen), mouse (n = 2 motor cortex; n = 2 striatum), and rat (n = 2 motor cortex, n = 2 striatum) using

bigWigMerge with default parameters. Combined bigwig files were examined using the Integrative Genomics Viewer (IGV), indexing using IGV's toTDF tool and group autoscaling tracks to ensure comparability of cortex and striatum open chromatin activity within species. Orthologous loci of either mouse- or human-derived enhancers were identified in other species using the BLAT web utility to map the original 'parent' enhancer sequence to each other species' genome. Given the variable length and orientation of mapped sequences, for comparative display we centered a 500 bp window around each peak, reversing sequences as needed to preserve the syntenic orientation relative to its closest gene observed in the parent sequence.

Stereotaxic implantation of optical fibers

Stereotaxic surgeries were performed in accordance with protocols approved by the Stanford Institutional Animal Care and Use Committee. Mice were maintained on a 12/12 light/dark cycle and fed ad libitum. All surgeries were carried out in aseptic conditions while mice were anaesthetized with isoflurane (5% for induction, 0.5%–1.5% afterward) in a manual stereotactic frame (Kopf). Buprenorphine HCl (0.1 mg kg-1, intraperotineal injection) and Ketoprofen (5 mg kg-1, subcutaneous injection) were used for postoperative analgesia. Mice were allowed to recover for at least 1 week before experiments. 200 mm fiber optic ferrules with 0.48 NA were implanted in the same surgery at coordinates +0.5mm AP, +/-1.5mm ML, -3.0mm DV.

Optogenetic stimulation

Mice were implanted unilaterally with fiber optic ferrules in dorsal striatum (injection coordinates: +/- 1.5 ML; +0.5 AP; -3.0 DV). Mice were tethered to flexible optical fibers connected to a fiber optic commutator (Doric Lenses). Optogenetic light stimulation was delivered with 10 s pulses of 450 mW green light at a 33% duty cycle and compared across three time windows: ''Pre'' (10 s prior to light onset), ''Light'' (10 s during light delivery), ''Post'' (10 s after light offset) over 30 repetitions for a total of 15 minutes. Equipment for LED light generation, optical fibers, and commutation were from Doric Lenses.

Tracking of locomotion in optogenetic stimulation

Mice were placed in a darkened, circular open arena 30 cm in diameter with a transparent floor illuminated from underneath with infrared LEDs. Video was acquired with a camera mounted underneath at 65 Hz. DeepLabCut was used to identify the nose and tail base of each mouse[89]. The average of these points was used to identify the center point for quantification of locomotor speed. The direction heading between these two points was used to identify rotations and change in direction. Rotations were quantified as a continuous 180°turn containing no more than 90 degrees of continuous rotation in the opposite direction.

Brain slice patch clamp electrophysiology

Enhancer AAV injected C57Bl6/J mice were deeply anaesthetized by intraperitoneal administration of Avertin (20 mg kg^{-1}) and were perfused through the heart with carbogenated (95% O_2/5% CO_2) artificial aCSF consisting of (in mM): 92 N-methyl-D-glucamine (NMDG), 2.5 KCl, 1.25 NaH_2PO_4, 30 $NaHCO_3$, 20 4-(2-hydroxyethyl)-1-piperazineethanesulfonic acid (HEPES), 25 glucose, 2 thiourea, 5 Na-ascorbate, 3 Na-pyruvate, 0.5 $CaCl_2 \cdot 4H_2O$ and 10 $MgSO_4 \cdot 7H_2O$. Brains were sliced at 300µm thickness on a vibratome (VT1200S, Leica Biosystems or Compresstome VF-300, Precisionary Instruments) using a zirconium ceramic blade and following the NMDG protective recovery method [Ting 2014]. Mouse brains were sectioned in the coronal plane such that the angle of slicing was perpendicular to the pial surface. After sections were obtained, slices were transferred to a warmed (32–34 °C) initial recovery chamber filled with NMDG aCSF under constant carbogenation. After 12 min, slices were transferred to a chamber containing HEPES holding aCSF solution consisting of (in mM): 92 NaCl, 2.5 KCl, 1.25 NaH2PO4, 30 NaHCO3, 20 HEPES, 25 glucose, 2 thiourea, 5 sodium

ascorbate, 3 sodium pyruvate, 2 CaCl2·4H2O and 2 MgSO4·7H2O, continuously bubbled with 95% O2/5% CO2. Slices were held in this chamber until use in acute patch clamp recordings or until fixed in 4% PFA for later histological processing.

Brain slices were placed in a submerged, heated (32-34°C) chamber that was continuously perfused with fresh, carbogenated aCSF consisting of (in mM): 119 NaCl, 2.5 KCl, 1.25 NaH_2PO_4, 24 $NaHCO_3$, 12.5 glucose, 2 $CaCl_2 \cdot 4H_2O$ and 2 $MgSO_4 \cdot 7H_2O$ (pH 7.3-7.4). Neurons were visualized with an upright microscope (Scientifica) equipped with infrared differential interference contrast (IR-DIC) optics and both 4x air and 40x water immersion objectives as well as epifluorescence illumination and filter cubes to detect SYFP2, mTFP1, and tdTomato fluorescence. Glass patch clamp pipettes were pulled to an open tip resistance of 2-6 MW when filled with the internal recording solution consisting of (in mM): 110.0 K-gluconate, 10.0 HEPES, 0.2 EGTA, 4 KCl, 0.3 Na_2-GTP, 10 phosphocreatine disodium salt hydrate, 1 Mg-ATP, 20 mg/mL glycogen, 0.5U/mL RNase inhibitor (Takara, 2313A), 0.5% biocytin and 0.02 Alexa 594 or 488 – pH adjusted to 7.3 with KOH. Whole cell somatic recordings were acquired using a Multiclamp 700B amplifier and custom acquisition software written in Igor Pro (MIES https://github.com/AllenInstitute/MIES. Electrical signals were digitized at 50 kHz by an ITC-18 (HEKA) and were filtered at 10 kHz. The pipette capacitance was compensated, and the bridge was balanced during the current clamp recordings.

Neurons were stimulated by injecting a sequence of 1s hyperpolarizing and depolarizing square wave current steps varying from -200pA to 450pA in 50pA increments. Intrinsic electrophysiological features were extracted using Python-based code adapted from Intrinsic Physiology Feature Extractor (IPFX, https://github.com/AllenInstitute/ipfx). Electrophysiological features used to cluster cells in 3D plots and highlight their physiological differences were calculated as follows: Frequency/Current (FI) Slope: calculated as the initial linear slope of the firing rate as a function of the current injection amplitude ; Steady-state input resistance: calculated from the linear fit of the current-voltage relationship measured in response to the series of hyperpolarizing steps; Upstroke/downstroke ratio: ratio of the maximum dVdt to the minimum dVdt for the first spike during the first current step that evoked spiking; Resting membrane potential: calculated as the membrane potential voltage with no current bias or current pulse injected; Action potential(AP) half-width: calculated as the duration of the action potential at the voltage halfway between AP threshold and the AP peak.

Macaque *in vivo* enhancer AAV injections

All procedures used with macaque monkeys conformed to the guidelines provided by the US National Institutes of Health and were approved by the University of Washington Animal Care and Use Committee. One 7 year old 5.8 kg female Southern pig-tailed macaque (*Macaca nemestrina*) was used in this study for *in vivo* injection of iodixanol gradient purified enhancer AAV vectors using the Brainsight® robotic injection system (Rogue Research). Brain MRI was acquired and utilized for pre-planning of virus injection surgery using the Brainsight® vet robot software v2.5. On the day of surgery, the animal was deeply anesthetized and positioned with the head in the stereotaxic frame of the Brainsight® surgery platform. A skin incision was made to expose the top of the skull, and burr hole craniotomies were drilled over the planned injection trajectory locations under the guidance of a robotic surgery arm. After craniotomy, a prefabricated steel cannula with PE tubing attachment[90] was loaded with a total of 15 µL AAV vector solution and attached to the robotic arm. A total of 5uL of virus was injected into caudate, and 5uL into putamen in two distinct injection tracks. For each track the cannula was advanced to the bottom of the injection target location and 1uL volume gradually injected at each of five depths with 1mm spacing as the cannula tip was retracted dorsally. At the end of the final injection site in each track, the cannula was left in place for 10 min prior to allow virus diffusion prior to removal from the brain. Note that additional virus injection sites were made in other distal brain locations in the same animal during the surgery.

At 36 days post-injection, the animal was sacrificed for brain collection and tissue expression analysis. The animal was perfused through the heart with 2L NMDG-aCSF solution and then the brain was removed and rapidly transported from the WaNPRC to the Allen Institute for further tissue processing. The brain was first hemisected and drop-fixed in freshly prepared 4% PFA in PBS for 48 hours at 4ºC. After PFA fixation, we transferred the brain into 1XPBS + 0.01% sodium azide solution. The brain hemispheres were examined and then 0.5 cm thick coronal slabs were cut through the striatum regions. Serial brain slabs were trimmed to fit into the wells of a six well tissue culture plate and submerged in 30% sucrose solution for a minimum of 48 hrs before further processing for histological analysis. Tissue slabs were mounted on the stage of a freezing-sliding microtome (Leica model SM2010R) on a bed of OCT and subsectioned to 30 µm thickness and stored in 1XPBS + 0.01% sodium azide solution. Sections in the region of interest were selected for PI and DAPI staining and then slide mounted on 2x3'' glass slides. Alternately, some tissue sections were used for free-floating immunostaining using the following antibodies: chicken anti-GFP IgY, mouse anti-DARPP32 IgG1, and mouse anti-ChAT IgG2b. Secondary antibodies were as follows: Alexa-488 conjugated goat anti-chicken IgGy (1:1000), Alexa-647 conjugated goat anti-mouse IgG1 (1:1000), and Alexa555-conjugated goat anti-mouse IgG2b (1:1000). Sections were dried onto slides on a slide warmer and coverslipped with Vectashield Hardset mounting medium (Vector Labs) for PI and DAPI plus native SYFP2 imaging or Prolong Gold Antifade mounting medium (Life Technologies) for antibody staining experiments. Please see 'Key Resource Table' for product details.

Data and materials availability:

Enhancer characterization data is available to view at the Allen Institute for Brain Science Genetic Tools Atlas (GTA):
https://portal.brain-map.org/genetic-tools/genetic-tools-atlas

All SSv4 scRNA-seq data have been deposited to the NeMO:
https://data.nemoarchive.org/other/grant/uf1_tasic/tasic/transcriptome/scell/SSv4/mouse/raw/

Primary screen epifluorescence and Serial-two-photon tomography (STPT) data are available at Brain Image Library (BIL) at: https://doi.brainimagelibrary.org/doi/10.35077/g.1159

Primary screen epifluorescence data can be found at BIL at:
https://download.brainimagelibrary.org/77/43/774317f96671fbd7/

Serial-two-photon tomography (STPT) data can be found at BIL at:
https://download.brainimagelibrary.org/07/7d/077dbfded4d55b5e/

Plasmid DNA for enhancer AAV vectors have been deposited to Addgene (see Key Resources table) as part of the NIH BRAIN Armamentarium collection (https://www.addgene.org/collections/brain-armamentarium/) and are available for distribution under standard UBMTA. mFISH data reported in this paper will be shared by the lead contact upon request. Any additional information required to reanalyze the data reported in this paper will be made available upon request.

Acknowledgements
We wish to thank the Allen Institute founder, Paul G. Allen, for his vision and the NIH BRAIN Initiative Armamentarium for Precision Brain Cell Access (https://braininitiative.nih.gov/armamentarium). This research was supported by U.S. National Institutes of Health (NIH) BRAIN Initiative Armamentarium Grant UF1MH128339 (BTa, JTT, BPL, TLD, and TEB) and in part by NIH BRAIN Initiative Human and Mammalian Brain Atlas (HMBA) BICAN grant UM1MH130981 (ESL, HZ), NIH grant R01MH123620 (BEK), and Allen Institute funding to the Genetic Tools project. We thank additional members of the core facilities and joint Brian Science shared resource teams including Laboratory Animal Services,

Transgenic Colony Management Team, Animal Care Team, Neurosurgery and Behavior Team, Viral Technology Team, Data and Technology Team, Histology Team, Imaging Team, Tissue Processing Team, Project Management Team, and Facilities Team. We thank the WaNPRC surgery and veterinary support staff and Chris English for necropsy support. The WaNPRC is supported by the NIH Office of Research Infrastructure Programs (ORIP) under award number P51OD010425 and U420D011123. We thank Dr. Elizabeth Buffalo for access to the BrainSight injection robot system and Megan Jutras for BrainSight support and training. We thank DISC lab and Tim Wilbur at the University of Washington for support with macaque MRI imaging. We thank TL Wong from the Kojima lab for support with fabricating virus injection cannulae and Shane Gibson from the Horwitz lab for support with macaque surgery and sample processing. Illustrations in Figure 6 were created with BioRender.com.

Author Contributions

Conceptualization: ACH, MEW, SFO, BPL, TLD, BT, TEB, JTT. Methodology: ACH, MEW, GG, NJJ, MH, VO, NT, NW, SV, JLB, BG, YB, XO, RAM, MNL, WL, SH, JKM, MJT, AW, ND, JA, YK, GH, SFO, BPL, TLD, BT, TEB, JTT. Software: MH, JRA, AA, CB, PB, ABC, RC, KC, SD, PD, TF, JG, ZH, NAL, ZM, JM, JM, EM, ALO, CR, DBR, LS, SS, YW, LN, BK. Validation: ACH, VO, NT, NW, SW, BT, JKM, SFO, BPL, TLD, BT, TEB, JTT. Formal Analysis: ACH, MEW, GG, NJJ, VO, NT, SV, YB, EM, SFO, JTT. Investigation: ACH, GG, VO, NT, NW, SV, JLB, BG, YB, MNL, WL, AA, AA, SB, DB, KB, NID, TE, AG, CG, WH, TJ, ZJ, JK, HL, JM, EM, RN, KN, KN, BO, AAO, TP, CP, LP, SR, CR, ARS, AR, MJT, MT, JW, JA, YK, GH, SFO, JTT. Resources: MEW, MH, XO, RAM, TB, JB, GB, BC, TC, MC, TD, MD, NPD, ELG, OH, WVH, CH, DLJ, ML, EL, RM, DN, ALO, NP, EP, MR, DFR, KR, JS, NVS, LS, TW, TZ, LE, SY, SM, KS, JW, IE, MP, JTT. Data curation: ACH, MEW, GG, NJJ, MH, SV, YB, SW, BT, MNL, WL, PMB, PB, DD, NAL, EM, IE, MP, SFO, BPL, TLD, JTT. Writing - original draft: ACH, MEW, GG, NJJ, SFO, JTT. Writing - review and editing: ACH, MEW, MJT, BK, SFO, BPL, TLD, BT, TEB, JTT Visualization: ACH, MEW, GG, NJJ, MH, SV, JLB, OS, RES, SD, SL, NAL, SM, CR, NS, BS, LN, SFO, JTT. Supervision: BG, YB, SH, MJT, AW, ND, LN, SY, JA, SM, KS, JW, HZ, ESL, YK, GH, SFO, BPL, TLD, BT, TEB, JTT. Project Administration: SW, BT, OS, RES, KG, TM, LE, IE, MP, GH, BPL, TLD, BT, TEB, JTT. Funding acquisition: BK, HZ, ESL, BPL, TLD, BT, TEB, JTT.

Declaration of interests

Authors JTT, BPL, EL, TLD, BTa, HZ, JKM are co-inventors on patent application PCT/US2021/45995 Artificial expression constructs for selectively modulating gene expression in striatal neurons. Authors JTT, BPL, TLD, BTa, TEB are co-inventors on provisional patent application US 63/582,759 Artificial expression constructs for modulating gene expression in the basal ganglia. HZ – is on the Scientific Advisory Board of MapLight Therapeutics, Palo Alto, CA

References

1. DeLong, M.R., and Wichmann, T. (2007). Circuits and circuit disorders of the basal ganglia. Arch. Neurol. *64*, 20–24.
2. Crittenden, J.R., and Graybiel, A.M. (2011). Basal Ganglia disorders associated with imbalances in the striatal striosome and matrix compartments. Front. Neuroanat. *5*, 59.
3. Lobo, M.K., and Nestler, E.J. (2011). The striatal balancing act in drug addiction: distinct roles of direct and indirect pathway medium spiny neurons. Front. Neuroanat. *5*, 41.
4. Lipton, D.M., Gonzales, B.J., and Citri, A. (2019). Dorsal striatal circuits for habits, compulsions and addictions. Front. Syst. Neurosci. *13*, 28.
5. Yasuo, and Kawaguchi (1993). Physiological, morphological, and histochemical characterization of three classes of interneurons in rat neostriatum. J. Neurosci. *13*, 4908–4923.
6. Gittis, A.H., Nelson, A.B., Thwin, M.T., Palop, J.J., and Kreitzer, A.C. (2010). Distinct roles of GABAergic interneurons in the regulation of striatal output pathways. J. Neurosci. *30*, 2223–2234.

7. Fino, E., Vandecasteele, M., Perez, S., Saudou, F., and Venance, L. (2018). Region-specific and state-dependent action of striatal GABAergic interneurons. Nat. Commun. *9*, 3339.
8. Assous, M., and Tepper, J.M. (2019). Excitatory extrinsic afferents to striatal interneurons and interactions with striatal microcircuitry. Eur. J. Neurosci. *49*, 593–603.
9. Gerfen, C.R., Paletzki, R., and Heintz, N. (2013). GENSAT BAC cre-recombinase driver lines to study the functional organization of cerebral cortical and basal ganglia circuits. Neuron *80*, 1368–1383.
10. Gong, S., Zheng, C., Doughty, M.L., Losos, K., Didkovsky, N., Schambra, U.B., Nowak, N.J., Joyner, A., Leblanc, G., Hatten, M.E., et al. (2003). A gene expression atlas of the central nervous system based on bacterial artificial chromosomes. Nature *425*, 917–925.
11. Gong, S., Doughty, M., Harbaugh, C.R., Cummins, A., Hatten, M.E., Heintz, N., and Gerfen, C.R. (2007). Targeting Cre recombinase to specific neuron populations with bacterial artificial chromosome constructs. J. Neurosci. *27*, 9817–9823.
12. Heiman, M., Schaefer, A., Gong, S., Peterson, J.D., Day, M., Ramsey, K.E., Suárez-Fariñas, M., Schwarz, C., Stephan, D.A., Surmeier, D.J., et al. (2008). A translational profiling approach for the molecular characterization of CNS cell types. Cell *135*, 738–748.
13. Shuen, J.A., Chen, M., Gloss, B., and Calakos, N. (2008). Drd1a-tdTomato BAC transgenic mice for simultaneous visualization of medium spiny neurons in the direct and indirect pathways of the basal ganglia. J. Neurosci. *28*, 2681–2685.
14. Tepper, J.M., Tecuapetla, F., Koós, T., and Ibáñez-Sandoval, O. (2010). Heterogeneity and diversity of striatal GABAergic interneurons. Front. Neuroanat. *4*, 150.
15. Tepper, J.M., Koós, T., Ibanez-Sandoval, O., Tecuapetla, F., Faust, T.W., and Assous, M. (2018). Heterogeneity and Diversity of Striatal GABAergic Interneurons: Update 2018. Front. Neuroanat. *12*, 91.
16. Dimidschstein, J., Chen, Q., Tremblay, R., Rogers, S.L., Saldi, G.-A., Guo, L., Xu, Q., Liu, R., Lu, C., Chu, J., et al. (2016). A viral strategy for targeting and manipulating interneurons across vertebrate species. Nat. Neurosci. *19*, 1743–1749.
17. Hrvatin, S., Tzeng, C.P., Nagy, M.A., Stroud, H., Koutsioumpa, C., Wilcox, O.F., Assad, E.G., Green, J., Harvey, C.D., Griffith, E.C., et al. (2019). A scalable platform for the development of cell-type-specific viral drivers. Elife *8*. https://doi.org/10.7554/eLife.48089.
18. Nair, R.R., Blankvoort, S., Lagartos, M.J., and Kentros, C. (2020). Enhancer-Driven Gene Expression (EDGE) enables the generation of viral vectors specific to neuronal subtypes. iScience *23*, 100888.
19. Vormstein-Schneider, D., Lin, J.D., Pelkey, K.A., Chittajallu, R., Guo, B., Arias-Garcia, M.A., Allaway, K., Sakopoulos, S., Schneider, G., Stevenson, O., et al. (2020). Viral manipulation of functionally distinct interneurons in mice, non-human primates and humans. Nat. Neurosci. *23*, 1629–1636.
20. Bakken, T.E., Jorstad, N.L., Hu, Q., Lake, B.B., Tian, W., Kalmbach, B.E., Crow, M., Hodge, R.D., Krienen, F.M., Sorensen, S.A., et al. (2021). Comparative cellular analysis of motor cortex in human, marmoset and mouse. Nature *598*, 111–119.
21. Graybuck, L.T., Daigle, T.L., Sedeño-Cortés, A.E., Walker, M., Kalmbach, B., Lenz, G.H., Morin, E., Nguyen, T.N., Garren, E., Bendrick, J.L., et al. (2021). Enhancer viruses for combinatorial cell-subclass-specific labeling. Neuron *109*, 1449-1464.e13.
22. Mich, J.K., Graybuck, L.T., Hess, E.E., Mahoney, J.T., Kojima, Y., Ding, Y., Somasundaram, S., Miller, J.A., Kalmbach, B.E., Radaelli, C., et al. (2021). Functional enhancer elements drive subclass-selective expression from mouse to primate neocortex. Cell Rep. *34*, 108754.
23. Krienen, F.M., Levandowski, K.M., Zaniewski, H., Del Rosario, R.C.H., Schroeder, M.E., Goldman, M., Wienisch, M., Lutservitz, A., Beja-Glasser, V.F., Chen, C., et al. (2023). A marmoset brain cell census reveals regional specialization of cellular identities. Sci. Adv. *9*, eadk3986.

24. Lee, B.R., Dalley, R., Miller, J.A., Chartrand, T., Close, J., Mann, R., Mukora, A., Ng, L., Alfiler, L., Baker, K., et al. (2023). Signature morphoelectric properties of diverse GABAergic interneurons in the human neocortex. Science *382*, eadf6484.
25. Mich, J.K., Sunil, S., Johansen, N., Martinez, R.A., Leytze, M., Gore, B.B., Mahoney, J.T., Ben-Simon, Y., Bishaw, Y., Brouner, K., et al. (2023). Enhancer-AAVs allow genetic access to oligodendrocytes and diverse populations of astrocytes across species. bioRxiv. https://doi.org/10.1101/2023.09.20.558718.
26. Furlanis, E., Dai, M., Garcia, B.L., Vergara, J., Pereira, A., Pelkey, K., Tran, T., Gorissen, B.L., Vlachos, A., Hairston, A., et al. (2024). An enhancer-AAV toolbox to target and manipulate distinct interneuron subtypes. bioRxivorg. https://doi.org/10.1101/2024.07.17.603924.
27. Gokce, O., Stanley, G.M., Treutlein, B., Neff, N.F., Camp, J.G., Malenka, R.C., Rothwell, P.E., Fuccillo, M.V., Südhof, T.C., and Quake, S.R. (2016). Cellular taxonomy of the mouse striatum as revealed by single-cell RNA-seq. Cell Rep. *16*, 1126–1137.
28. Muñoz-Manchado, A.B., Bengtsson Gonzales, C., Zeisel, A., Munguba, H., Bekkouche, B., Skene, N.G., Lönnerberg, P., Ryge, J., Harris, K.D., Linnarsson, S., et al. (2018). Diversity of Interneurons in the Dorsal Striatum Revealed by Single-Cell RNA Sequencing and PatchSeq. Cell Rep. *24*, 2179-2190.e7.
29. Saunders, A., Macosko, E.Z., Wysoker, A., Goldman, M., Krienen, F.M., de Rivera, H., Bien, E., Baum, M., Bortolin, L., Wang, S., et al. (2018). Molecular Diversity and Specializations among the Cells of the Adult Mouse Brain. Cell *174*, 1015-1030.e16.
30. Yao, Z., van Velthoven, C.T.J., Kunst, M., Zhang, M., McMillen, D., Lee, C., Jung, W., Goldy, J., Abdelhak, A., Aitken, M., et al. (2023). A high-resolution transcriptomic and spatial atlas of cell types in the whole mouse brain. Nature *624*, 317–332.
31. Krienen, F.M., Goldman, M., Zhang, Q., C H Del Rosario, R., Florio, M., Machold, R., Saunders, A., Levandowski, K., Zaniewski, H., Schuman, B., et al. (2020). Innovations present in the primate interneuron repertoire. Nature *586*, 262–269.
32. He, J., Kleyman, M., Chen, J., Alikaya, A., Rothenhoefer, K.M., Ozturk, B.E., Wirthlin, M.E., Bostan, A.C., Fish, K., Byrne, L., et al. (2021). Transcriptional and anatomical diversity of medium spiny neurons in the primate striatum. Curr. Biol. *31*, 5473-5486.e6.
33. Siletti, K., Hodge, R., Mossi Albiach, A., Lee, K.W., Ding, S.-L., Hu, L., Lönnerberg, P., Bakken, T., Casper, T., Clark, M., et al. (2023). Transcriptomic diversity of cell types across the adult human brain. Science *382*, eadd7046.
34. Garma, L.D., Harder, L., Barba-Reyes, J.M., Marco Salas, S., Díez-Salguero, M., Nilsson, M., Serrano-Pozo, A., Hyman, B.T., and Muñoz-Manchado, A.B. (2024). Interneuron diversity in the human dorsal striatum. Nat. Commun. *15*, 6164.
35. Fullard, J.F., Hauberg, M.E., Bendl, J., Egervari, G., Cirnaru, M.-D., Reach, S.M., Motl, J., Ehrlich, M.E., Hurd, Y.L., and Roussos, P. (2018). An atlas of chromatin accessibility in the adult human brain. Genome Res. *28*, 1243–1252.
36. Li, Y.E., Preissl, S., Hou, X., Zhang, Z., Zhang, K., Qiu, Y., Poirion, O.B., Li, B., Chiou, J., Liu, H., et al. (2021). An atlas of gene regulatory elements in adult mouse cerebrum. Nature *598*, 129–136.
37. Zu, S., Li, Y.E., Wang, K., Armand, E.J., Mamde, S., Amaral, M.L., Wang, Y., Chu, A., Xie, Y., Miller, M., et al. (2023). Single-cell analysis of chromatin accessibility in the adult mouse brain. Nature *624*, 378–389.
38. Kremers, G.-J., Goedhart, J., van Munster, E.B., and Gadella, T.W.J., Jr (2006). Cyan and yellow super fluorescent proteins with improved brightness, protein folding, and FRET Förster radius'. Biochemistry *45*, 6570–6580.
39. Chan, K.Y., Jang, M.J., Yoo, B.B., Greenbaum, A., Ravi, N., Wu, W.-L., Sánchez-Guardado, L., Lois, C., Mazmanian, S.K., Deverman, B.E., et al. (2017). Engineered AAVs for efficient noninvasive gene delivery to the central and peripheral nervous systems. Nat. Neurosci. *20*, 1172–1179.

40. Bateup, H.S., Svenningsson, P., Kuroiwa, M., Gong, S., Nishi, A., Heintz, N., and Greengard, P. (2008). Cell type-specific regulation of DARPP-32 phosphorylation by psychostimulant and antipsychotic drugs. Nat. Neurosci. *11*, 932–939.
41. Lanciego, J.L., Luquin, N., and Obeso, J.A. (2012). Functional neuroanatomy of the basal ganglia. Cold Spring Harb. Perspect. Med. *2*, a009621.
42. Kawaguchi, Y., Wilson, C.J., Augood, S.J., and Emson, P.C. (1995). Striatal interneurones: chemical, physiological and morphological characterization. Trends Neurosci. *18*, 527–535.
43. Kawaguchi, Y. (1997). Neostriatal cell subtypes and their functional roles. Neurosci. Res. *27*, 1–8.
44. Marin, O., Anderson, S.A., and Rubenstein, J.L. (2000). Origin and molecular specification of striatal interneurons. J. Neurosci. *20*, 6063–6076.
45. Ben-Simon, Y., Hooper, M., Narayan, S., Daigle, T., Dwivedi, D., Way, S.W., Oster, A., Stafford, D.A., Mich, J.K., Taormina, M.J., et al. (2024). A suite of enhancer AAVs and transgenic mouse lines for genetic access to cortical cell types. bioRxivorg. https://doi.org/10.1101/2024.06.10.597244.
46. Martel, A.-C., Elseedy, H., Lavigne, M., Scapula, J., Ghestem, A., Kremer, E.J., Esclapez, M., and Apicella, P. (2020). Targeted transgene expression in cholinergic interneurons in the monkey striatum using canine Adenovirus serotype 2 vectors. Front. Mol. Neurosci. *13*, 76.
47. Santoscoy, M.C., Espinoza, P., De La Cruz, D., Mahamdeh, M., Starr, J.R., Patel, N., and Maguire, C.A. (2023). An AAV capsid increases transduction of striatum and a ChAT promoter allows selective cholinergic neuron transduction. Mol. Ther. Methods Clin. Dev. *29*, 532–540.
48. Kawaguchi, Y., Wilson, C.J., and Emson, P.C. (1990). Projection subtypes of rat neostriatal matrix cells revealed by intracellular injection of biocytin. J. Neurosci. *10*, 3421–3438.
49. Cui, Q., Du, X., Chang, I.Y.M., Pamukcu, A., Lilascharoen, V., Berceau, B.L., García, D., Hong, D., Chon, U., Narayanan, A., et al. (2021). Striatal direct pathway targets Npas1+ pallidal neurons. J. Neurosci. *41*, 3966–3987.
50. Hartung, M., and Kisters-Woike, B. (1998). Cre mutants with altered DNA binding properties. J. Biol. Chem. *273*, 22884–22891.
51. Tsien, J.Z., Chen, D.F., Gerber, D., Tom, C., Mercer, E.H., Anderson, D.J., Mayford, M., Kandel, E.R., and Tonegawa, S. (1996). Subregion- and cell type-restricted gene knockout in mouse brain. Cell *87*, 1317–1326.
52. Madisen, L., Zwingman, T.A., Sunkin, S.M., Oh, S.W., Zariwala, H.A., Gu, H., Ng, L.L., Palmiter, R.D., Hawrylycz, M.J., Jones, A.R., et al. (2010). A robust and high-throughput Cre reporting and characterization system for the whole mouse brain. Nat. Neurosci. *13*, 133–140.
53. Durieux, P.F., Bearzatto, B., Guiducci, S., Buch, T., Waisman, A., Zoli, M., Schiffmann, S.N., and de Kerchove d'Exaerde, A. (2009). D2R striatopallidal neurons inhibit both locomotor and drug reward processes. Nat. Neurosci. *12*, 393–395.
54. Krashes, M.J., Shah, B.P., Madara, J.C., Olson, D.P., Strochlic, D.E., Garfield, A.S., Vong, L., Pei, H., Watabe-Uchida, M., Uchida, N., et al. (2014). An excitatory paraventricular nucleus to AgRP neuron circuit that drives hunger. Nature *507*, 238–242.
55. Prigge, M., Schneider, F., Tsunoda, S.P., Shilyansky, C., Wietek, J., Deisseroth, K., and Hegemann, P. (2012). Color-tuned channelrhodopsins for multiwavelength optogenetics. J. Biol. Chem. *287*, 31804–31812.
56. Assous, M., Faust, T.W., Assini, R., Shah, F., Sidibe, Y., and Tepper, J.M. (2018). Identification and characterization of a novel spontaneously active bursty GABAergic interneuron in the mouse striatum. J. Neurosci. *38*, 5688–5699.
57. Klapoetke, N.C., Murata, Y., Kim, S.S., Pulver, S.R., Birdsey-Benson, A., Cho, Y.K., Morimoto, T.K., Chuong, A.S., Carpenter, E.J., Tian, Z., et al. (2014). Independent optical excitation of distinct neural populations. Nat. Methods *11*, 338–346.
58. Zhang, Y., Rózsa, M., Liang, Y., Bushey, D., Wei, Z., Zheng, J., Reep, D., Broussard, G.J., Tsang, A., Tsegaye, G., et al. (2023). Fast and sensitive GCaMP calcium indicators for imaging neural populations. Nature *615*, 884–891.

59. Tervo, D.G.R., Hwang, B.-Y., Viswanathan, S., Gaj, T., Lavzin, M., Ritola, K.D., Lindo, S., Michael, S., Kuleshova, E., Ojala, D., et al. (2016). A designer AAV variant permits efficient retrograde access to projection neurons. Neuron *92*, 372–382.
60. Lin, K., Zhong, X., Li, L., Ying, M., Yang, T., Zhang, Z., He, X., and Xu, F. (2020). AAV9-Retro mediates efficient transduction with axon terminal absorption and blood-brain barrier transportation. Mol. Brain *13*, 138.
61. Day, M., Wokosin, D., Plotkin, J.L., Tian, X., and Surmeier, D.J. (2008). Differential excitability and modulation of striatal medium spiny neuron dendrites. J. Neurosci. *28*, 11603–11614.
62. Gertler, T.S., Chan, C.S., and Surmeier, D.J. (2008). Dichotomous anatomical properties of adult striatal medium spiny neurons. J. Neurosci. *28*, 10814–10824.
63. Kravitz, A.V., Freeze, B.S., Parker, P.R.L., Kay, K., Thwin, M.T., Deisseroth, K., and Kreitzer, A.C. (2010). Regulation of parkinsonian motor behaviours by optogenetic control of basal ganglia circuitry. Nature *466*, 622–626.
64. Kravitz, A.V., Tye, L.D., and Kreitzer, A.C. (2012). Distinct roles for direct and indirect pathway striatal neurons in reinforcement. Nat. Neurosci. *15*, 816–818.
65. Nelson, A.B., and Kreitzer, A.C. (2014). Reassessing models of basal ganglia function and dysfunction. Annu. Rev. Neurosci. *37*, 117–135.
66. Klaus, A., Alves da Silva, J., and Costa, R.M. (2019). What, if, and when to move: Basal ganglia circuits and self-paced action initiation. Annu. Rev. Neurosci. *42*, 459–483.
67. Gerfen, C.R., Engber, T.M., Mahan, L.C., Susel, Z., Chase, T.N., Monsma, F.J., Jr, and Sibley, D.R. (1990). D1 and D2 dopamine receptor-regulated gene expression of striatonigral and striatopallidal neurons. Science *250*, 1429–1432.
68. Gore, B.B., and Zweifel, L.S. (2013). Genetic reconstruction of dopamine D1 receptor signaling in the nucleus accumbens facilitates natural and drug reward responses. J. Neurosci. *33*, 8640–8649.
69. Juarez, B., Morel, C., Ku, S.M., Liu, Y., Zhang, H., Montgomery, S., Gregoire, H., Ribeiro, E., Crumiller, M., Roman-Ortiz, C., et al. (2017). Midbrain circuit regulation of individual alcohol drinking behaviors in mice. Nat. Commun. *8*, 2220.
70. Phillips, R.A., 3rd, Tuscher, J.J., Fitzgerald, N.D., Wan, E., Zipperly, M.E., Duke, C.G., Ianov, L., and Day, J.J. (2023). Distinct subpopulations of D1 medium spiny neurons exhibit unique transcriptional responsiveness to cocaine. Mol. Cell. Neurosci. *125*, 103849.
71. He, M., Tucciarone, J., Lee, S., Nigro, M.J., Kim, Y., Levine, J.M., Kelly, S.M., Krugikov, I., Wu, P., Chen, Y., et al. (2016). Strategies and tools for combinatorial targeting of GABAergic neurons in mouse cerebral cortex. Neuron *91*, 1228–1243.
72. Daigle, T.L., Madisen, L., Hage, T.A., Valley, M.T., Knoblich, U., Larsen, R.S., Takeno, M.M., Huang, L., Gu, H., Larsen, R., et al. (2018). A suite of transgenic driver and reporter mouse lines with enhanced brain-cell-type targeting and functionality. Cell *174*, 465-480.e22.
73. Witten, I.B., Steinberg, E.E., Lee, S.Y., Davidson, T.J., Zalocusky, K.A., Brodsky, M., Yizhar, O., Cho, S.L., Gong, S., Ramakrishnan, C., et al. (2011). Recombinase-driver rat lines: tools, techniques, and optogenetic application to dopamine-mediated reinforcement. Neuron *72*, 721–733.
74. Bäck, S., Necarsulmer, J., Whitaker, L.R., Coke, L.M., Koivula, P., Heathward, E.J., Fortuno, L.V., Zhang, Y., Yeh, C.G., Baldwin, H.A., et al. (2019). Neuron-specific genome modification in the adult rat brain using CRISPR-Cas9 transgenic rats. Neuron *102*, 105-119.e8.
75. Kaspar, B.K., Vissel, B., Bengoechea, T., Crone, S., Randolph-Moore, L., Muller, R., Brandon, E.P., Schaffer, D., Verma, I.M., Lee, K.-F., et al. (2002). Adeno-associated virus effectively mediates conditional gene modification in the brain. Proc. Natl. Acad. Sci. U. S. A. *99*, 2320–2325.
76. Luo, L., Ambrozkiewicz, M.C., Benseler, F., Chen, C., Dumontier, E., Falkner, S., Furlanis, E., Gomez, A.M., Hoshina, N., Huang, W.-H., et al. (2020). Optimizing nervous system-specific gene targeting with Cre driver lines: Prevalence of germline recombination and influencing factors. Neuron *106*, 37-65.e5.

77. Hunker, A.C., Soden, M.E., Krayushkina, D., Heymann, G., Awatramani, R., and Zweifel, L.S. (2020). Conditional single vector CRISPR/SaCas9 viruses for efficient Mutagenesis in the adult mouse nervous system. Cell Rep. *30*, 4303-4316.e6.
78. Moffa, J.C., Bland, I.N., Tooley, J.R., Kalyanaraman, V., Heitmeier, M., Creed, M.C., and Copits, B.A. (2023). Cell specific single viral vector CRISPR/Cas9 editing and genetically encoded tool delivery in the central and peripheral nervous systems. bioRxivorg. https://doi.org/10.1101/2023.10.10.561249.
79. Ramani, B., Rose, I.V.L., Pan, A., Tian, R., Ma, K., Palop, J.J., and Kampmann, M. (2023). Scalable, cell type-selective, AAV-based in vivo CRISPR screening in the mouse brain. bioRxivorg. https://doi.org/10.1101/2023.06.13.544831.
80. Kravitz, A.V., Owen, S.F., and Kreitzer, A.C. (2013). Optogenetic identification of striatal projection neuron subtypes during in vivo recordings. Brain Res. *1511*, 21–32.
81. Shin, J.H., Kim, D., and Jung, M.W. (2018). Differential coding of reward and movement information in the dorsomedial striatal direct and indirect pathways. Nat. Commun. *9*, 404.
82. Li, H., and Jin, X. (2023). Multiple dynamic interactions from basal ganglia direct and indirect pathways mediate action selection. Elife *12*. https://doi.org/10.7554/eLife.87644.
83. Coughlin, G.M., Borsos, M., Appling, N., Barcelona, B.H., Mayfield, A.M.H., Mackey, E.D., Eser, R.A., Chen, X., Kumar, S.R., and Gradinaru, V. (2023). Spatial genomics of AAVs reveals mechanism of transcriptional crosstalk that enables targeted delivery of large genetic cargo. bioRxivorg. https://doi.org/10.1101/2023.12.23.573214.
84. Ng, L., Bernard, A., Lau, C., Overly, C.C., Dong, H.-W., Kuan, C., Pathak, S., Sunkin, S.M., Dang, C., Bohland, J.W., et al. (2009). An anatomic gene expression atlas of the adult mouse brain. Nat. Neurosci. *12*, 356–362.
85. Zhang, K., Hocker, J.D., Miller, M., Hou, X., Chiou, J., Poirion, O.B., Qiu, Y., Li, Y.E., Gaulton, K.J., Wang, A., et al. (2021). A single-cell atlas of chromatin accessibility in the human genome. Cell *184*, 5985-6001.e19.
86. Guo, C., Kong, W., Kamimoto, K., Rivera-Gonzalez, G.C., Yang, X., Kirita, Y., and Morris, S.A. (2019). CellTag Indexing: genetic barcode-based sample multiplexing for single-cell genomics. Genome Biol. *20*, 90.
87. Bankhead, P., Loughrey, M.B., Fernández, J.A., Dombrowski, Y., McArt, D.G., Dunne, P.D., McQuaid, S., Gray, R.T., Murray, L.J., Coleman, H.G., et al. (2017). QuPath: Open source software for digital pathology image analysis. Sci. Rep. *7*, 16878.
88. Tasic, B., Yao, Z., Graybuck, L.T., Smith, K.A., Nguyen, T.N., Bertagnolli, D., Goldy, J., Garren, E., Economo, M.N., Viswanathan, S., et al. (2018). Shared and distinct transcriptomic cell types across neocortical areas. Nature *563*, 72–78.
89. Mathis, A., Mamidanna, P., Cury, K.M., Abe, T., Murthy, V.N., Mathis, M.W., and Bethge, M. (2018). DeepLabCut: markerless pose estimation of user-defined body parts with deep learning. Nature neuroscience *21*, 1281–1289.
90. Kojima, Y., Ting, J.T., Soetedjo, R., Gibson, S.D., and Horwitz, G.D. (2021). Injections of AAV vectors for optogenetics in anesthetized and awake behaving non-human primate brain. J. Vis. Exp. https://doi.org/10.3791/62546.

Figure 1

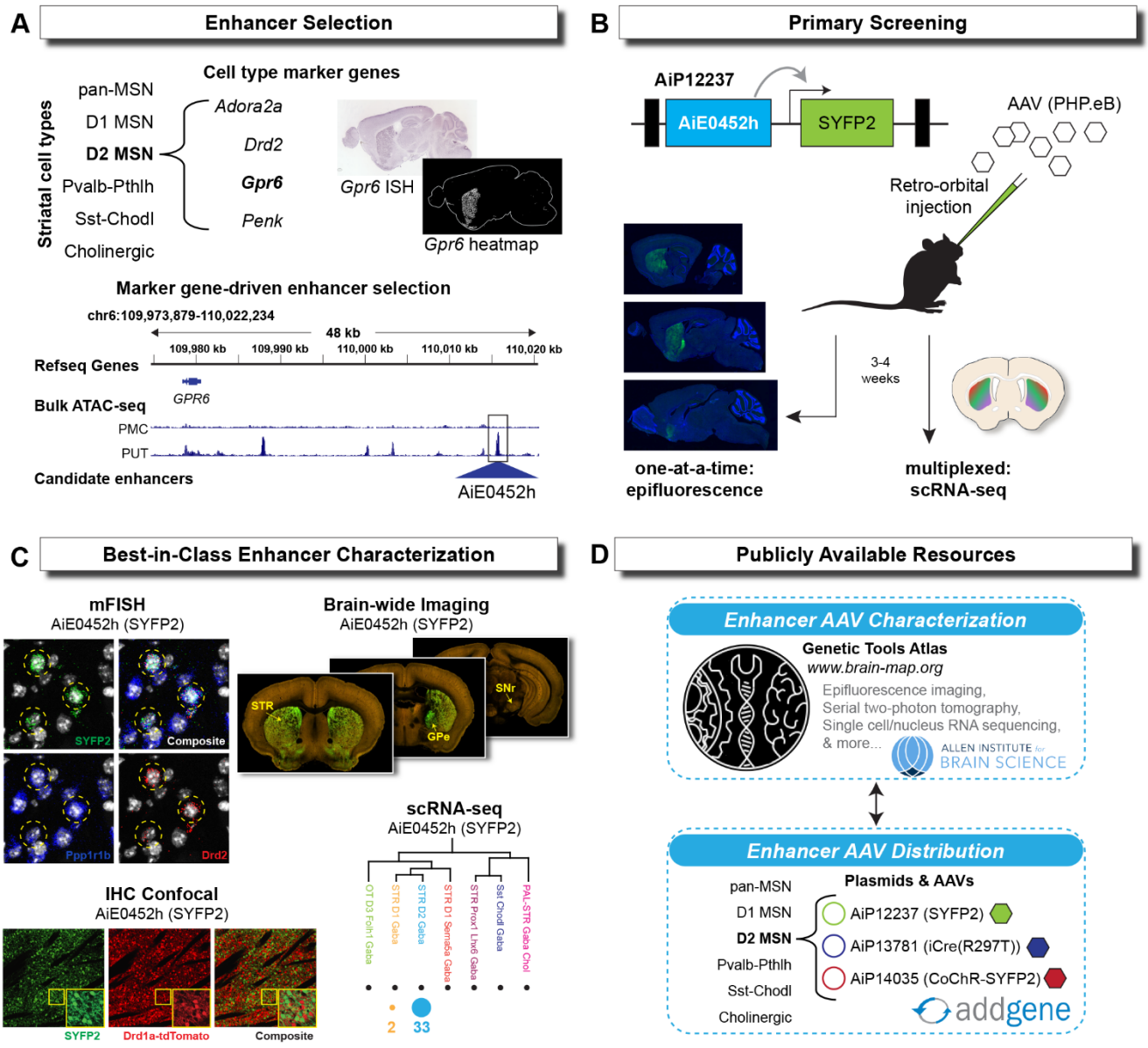

Figure 1. Pipeline for the discovery, validation, and distribution of striatal enhancer AAVs. A) Diagram of enhancer selection process. Isolated peaks are chosen based on proximity to marker genes from multiple different ATAC-seq datasets. B) Putative enhancer sequences were screened for cell type specific activity by retro-orbital injection using SYFP2 native fluorescence. Example shown is of plasmid AiP12237 that contains the D2 MSN enhancer AiE0452h driving expression of SYFP2. C) The most promising "Best-in-Class" enhancers were further validated for on-target activity by comparing mRNA and protein expression across multiple techniques. D) Striatal enhancer AAV characterization data is publicly available through the Allen Institute for Brain Science Genetic Tools Atlas (https://portal.brain-map.org/genetic-tools/genetic-tools-atlas). Enhancer AAV plasmid DNA and select virus aliquots are available from Addgene for distribution to the research community.

Figure 2

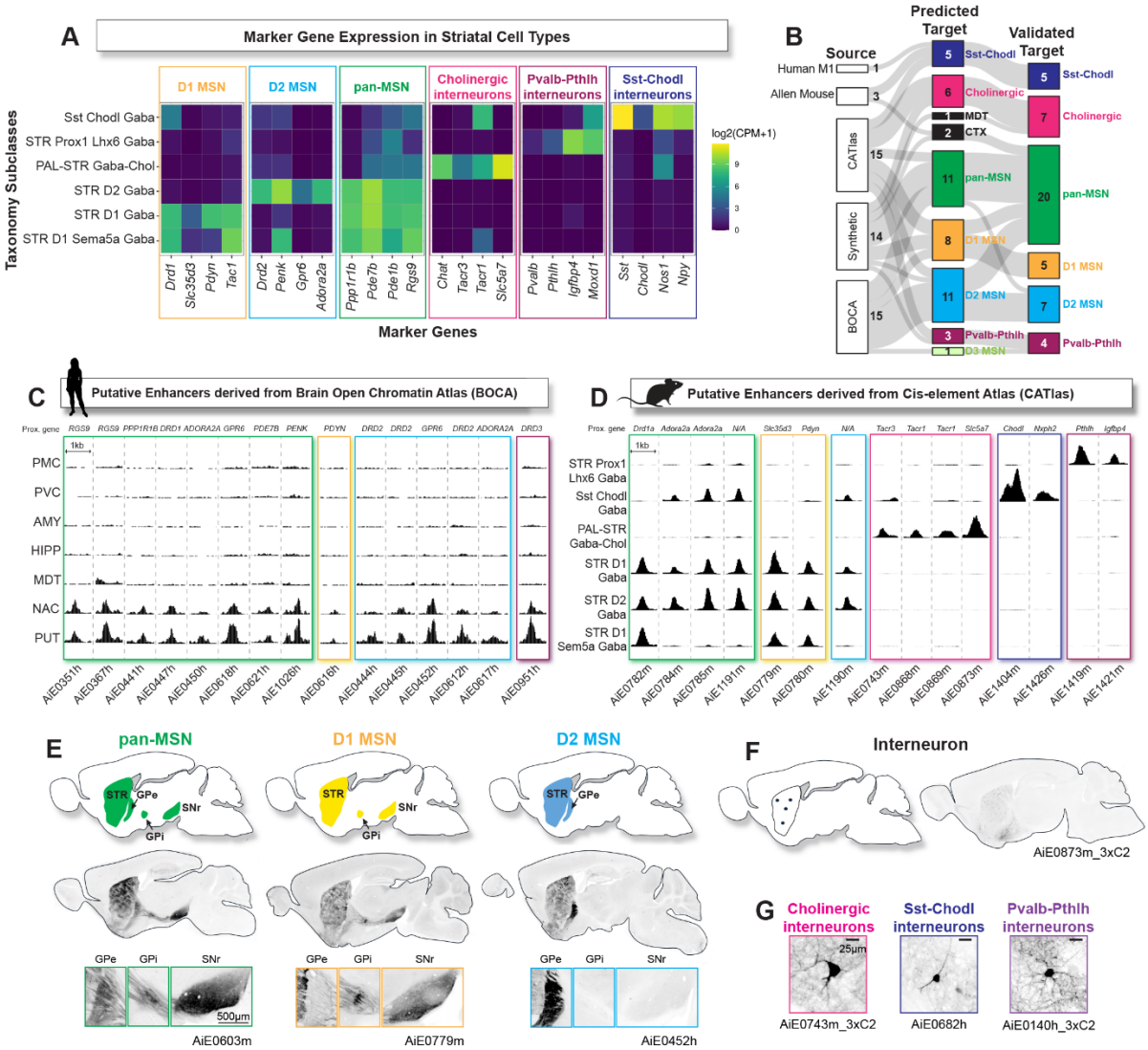

Figure 2. Putative enhancers can drive cell type specific expression in the striatum. A) Heatmap of median transcript detection log2(CPM+1) of striatal cell type marker genes from CCN20230722 mouse whole brain taxonomy cluster matrix. Colored boxes group marker genes by corresponding cell type common name. B) Sankey diagram with three nodes indicating the sources for all putative enhancer peaks for each cell target, their predicted expression specificities, and their validated expression. Values indicate number of enhancers at each node. C-D) Putative enhancer peaks selected for striatal cell types from BOCA (C) and CATlas (D) datasets. Tracks are grouped by brain region for BOCA (PMC: primary motor cortex, PVC: primary visual cortex, AMY: amygdala, HIPP: hippocampus, MDT: medio-dorsal thalamus, NAC: nucleus accumbens, PUT: putamen) and by CCN20230722 whole mouse brain taxonomy designated cell subclass for CATlas. The marker gene each peak was found proximal to is noted above each peak (N/A indicates peak was not found near any known marker gene). Enhancer peaks are grouped by target (gold: D1 MSN, turquoise: D2 MSN, green: pan-MSN, pink: cholinergic interneurons, dark blue: Sst-Chodl interneurons. Maroon: Pvalb-Pthlh interneurons. E) Top: diagram of expression patterns indicative of striatal MSN cell populations. Middle: example sagittal sections of native SYFP2 expression from enhancer AAVs for each indicated MSN population. Bottom: zoomed in views of axonal projection patterns in basal ganglia target regions from the same enhancer AAV as middle panel (GPi: globus pallidus internal segment, GPe: globus pallidus external segment, SNr: substantia nigra pars reticulata). F) Left: diagram of expression patterns indicative of striatal interneuron populations. Right: example sagittal section of native SYFP2 from enhancer AAV with interneuron expression selectivity. G) Example of morphological differences for distinguishing striatal interneuron populations. Note large size of cholinergic interneuron somata and thick dendrite caliber, elongated or bipolar Sst-Chodl interneurons with thin dendrite caliber, and compact dendrites of multipolar Pvalb-Pthlh interneurons.

Figure 3

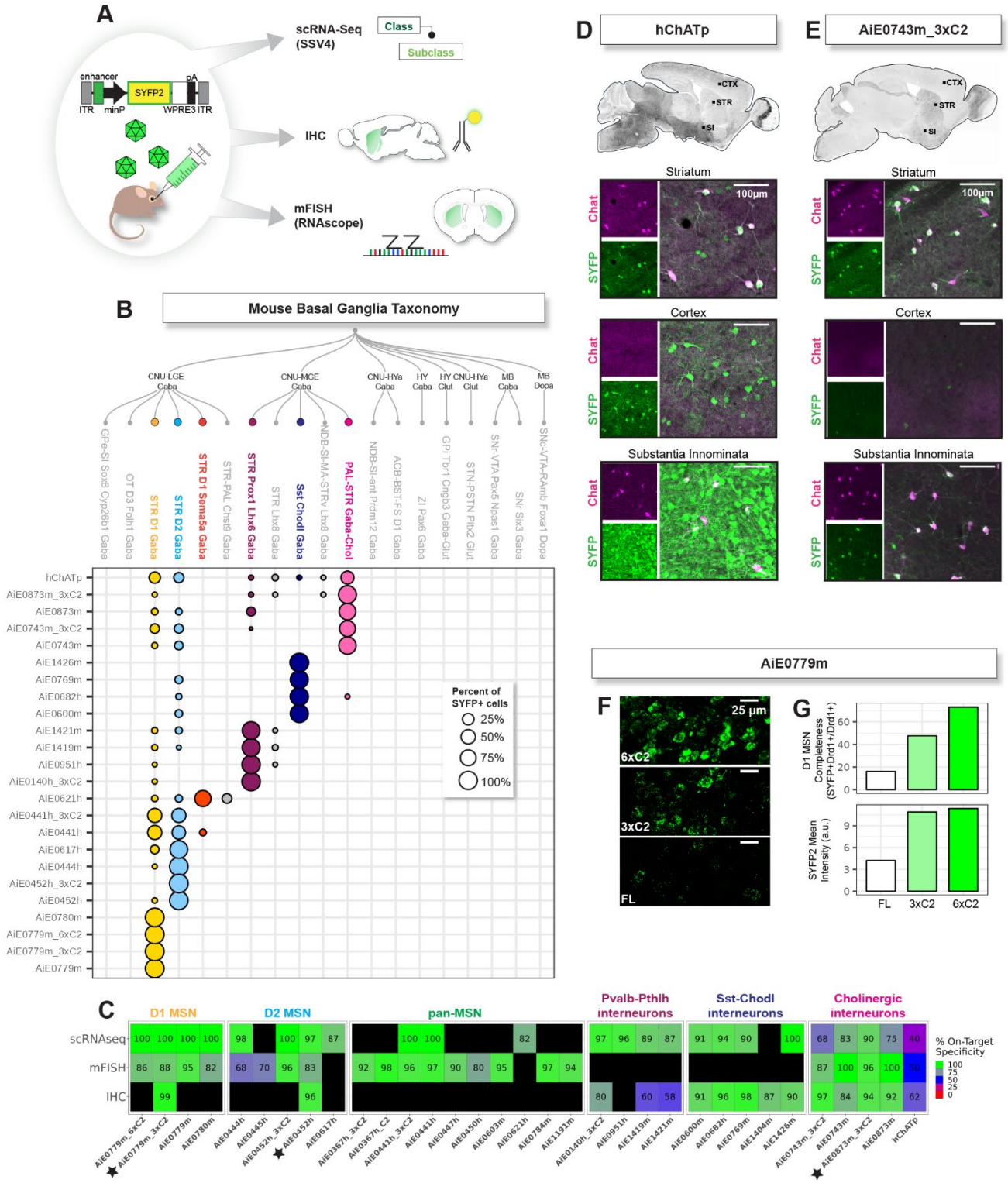
A
scRNA-Seq (SSV4)
Class
Subclass
enhancer
SYFP2
pA
ITR
minP
WPRE3
ITR
IHC
mFISH (RNAscope)
B
Mouse Basal Ganglia Taxonomy
CNU-LGE Gaba
CNU-MGE Gaba
CNU-HYa Gaba
HY Gaba
HY Glut
CNU-HYa Glut
MB Gaba
MB Dopa
GPe-SI Sox6 Cyp26b1 Gaba
OT D3 Foxb1 Gaba
STR D1 Gaba
STR D2 Gaba
STR D1 Sema5a Gaba
STR-PAL Chst9 Gaba
STR Prox1 Lhx6 Gaba
STR Lhx8 Gaba
Sst Chodl Gaba
NDB-SI-MA-STRv Lhx8 Gaba
PAL-STR Gaba-Chol
NDB-SI-ant Prdm12 Gaba
ACB-BST-FS D1 Gaba
ZI Pax6 Gaba
GPi Tbr1 Cnga3 Gaba-Glut
STN-PSTN Pitx2 Glut
SNr-VTA Pax5 Npas1 Gaba
SNr Six3 Gaba
SNc-VTA-RAmb Foxa1 Dopa
hChATp
AiE0873m_3xC2
AiE0873m
AiE0743m_3xC2
AiE0743m
AiE1426m
AiE0769m
AiE0682h
AiE0600m
AiE1421m
AiE1419m
AiE0951h
AiE0140h_3xC2
AiE0621h
AiE0441h_3xC2
AiE0441h
AiE0617h
AiE0444h
AiE0452h_3xC2
AiE0452h
AiE0780m
AiE0779m_6xC2
AiE0779m_3xC2
AiE0779m
Percent of SYFP+ cells
25%
50%
75%
100%
D
hChATp
E
AiE0743m_3xC2
CTX
STR
SI
Striatum
Cortex
Substantia Innominata
Chat
SYFP
100µm
AiE0779m
F
25 µm
6xC2
3xC2
FL
G
D1 MSN Completeness (SYFP+Drd1+/Drd1+)
SYFP2 Mean Intensity (a.u.)
FL
3xC2
6xC2
C
D1 MSN
D2 MSN
pan-MSN
Pvalb-Pthlh interneurons
Sst-Chodl interneurons
Cholinergic interneurons
scRNAseq
mFISH
IHC
% On-Target Specificity
100
75
50
25
0

Figure 3. Striatal enhancer AAVs demonstrate significant improvement in cell type specificity over existing tools. A) Diagram of triple modality enhancer AAV validation process including scRNA-seq (Smart-seq V4, SSv4), immunohistochemistry (IHC), and mFISH (RNAscope). B) Enhancer specificities determined by SSv4 scRNA-seq. Sequenced transcriptomes were mapped against the 10X Whole Mouse Brain taxonomy CCN20230722 using hierarchical mapping algorithm in MapMyCells (Allen Brain Map). Cell types in dendrogram encompass all neuronal basal ganglia subclasses from the taxonomy, with the six cell types targeted in this manuscript highlighted in color.C) Quantification of on-target enhancer AAV specificities across all three validation methods. Black boxes indicate no data and stars indicate 3 of the top enhancers. D-E) Top: example sagittal sections of hChATp (D) or AiE0743m_3xC2 (E)-driven native SYFP2 fluorescence. Bottom: Identification of striatal cholinergic interneurons by IHC using ChAT subclass marker antibody. Each panel is a representative ROI from three different brain regions. D) F) RNAscope using probes against SYFP2 for three versions of the AiE0779m D1 MSN enhancer. G) Quantification of completeness and signal intensity from RNAscope images.

Figure 4

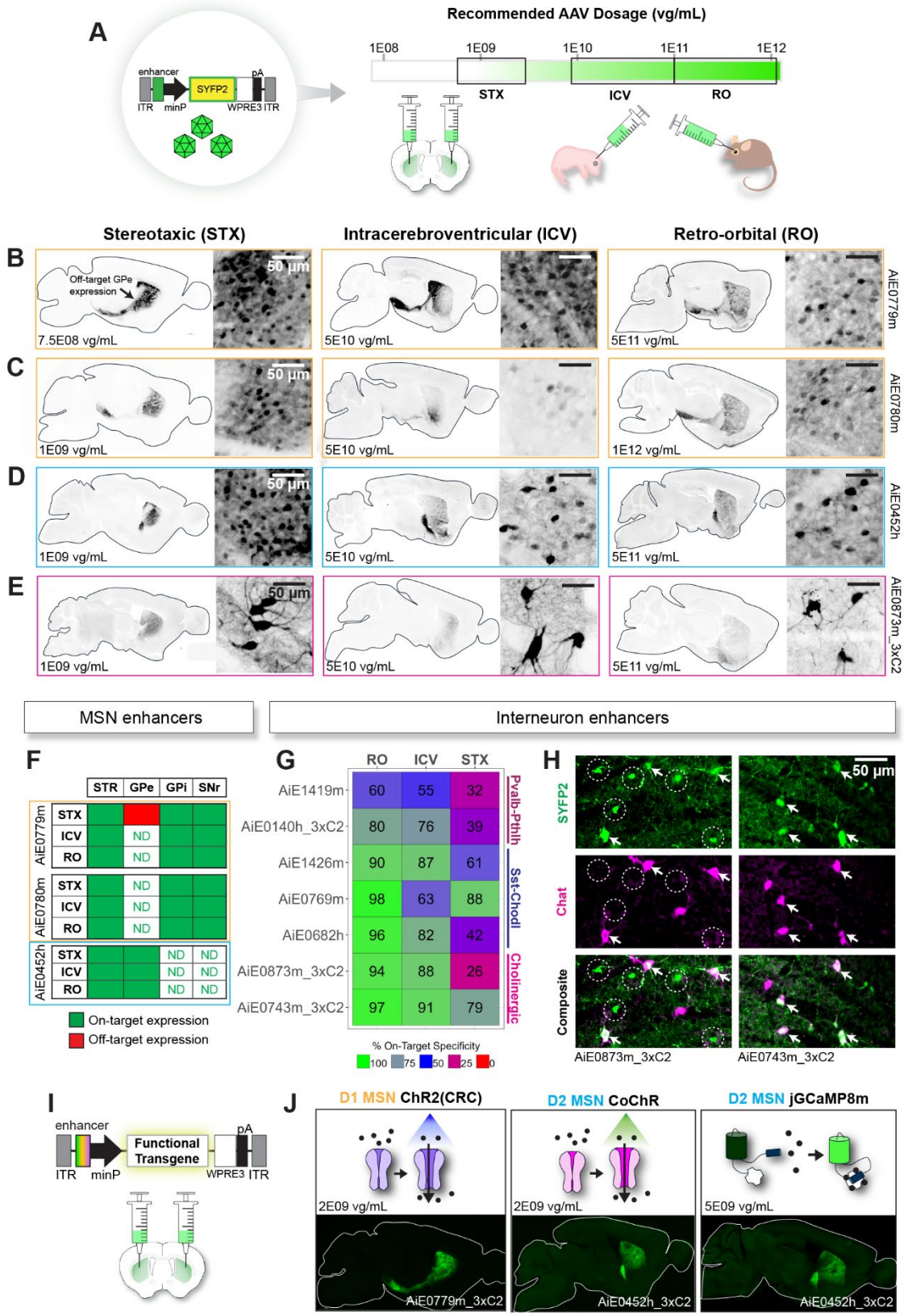
A
enhancer
SYFP2
pA
ITR
minP
WPRE3
ITR
Recommended AAV Dosage (vg/mL)
1E08
1E09
1E10
1E11
1E12
STX
ICV
RO
Stereotaxic (STX)
Intracerebroventricular (ICV)
Retro-orbital (RO)
B
Off-target GPe expression
50 µm
7.5E08 vg/mL
5E10 vg/mL
5E11 vg/mL
AiE0779m
C
1E09 vg/mL
5E10 vg/mL
1E12 vg/mL
AiE0780m
D
1E09 vg/mL
5E10 vg/mL
5E11 vg/mL
AiE0452h
E
1E09 vg/mL
5E10 vg/mL
5E11 vg/mL
AiE0873m_3xC2
MSN enhancers
Interneuron enhancers
F
STR
GPe
GPi
SNr
AiE0779m
STX
ICV
RO
ND
AiE0780m
AiE0452h
On-target expression
Off-target expression
G
RO
ICV
STX
AiE1419m
AiE0140h_3xC2
AiE1426m
AiE0769m
AiE0682h
AiE0873m_3xC2
AiE0743m_3xC2
Pvalb-Pthlh
Sst-Chodl
Cholinergic
% On-Target Specificity
100
75
50
25
0
H
SYFP2
Chat
Composite
AiE0873m_3xC2
AiE0743m_3xC2
I
enhancer
Functional Transgene
pA
ITR
minP
WPRE3
ITR
J
D1 MSN ChR2(CRC)
D2 MSN CoChR
D2 MSN jGCaMP8m
2E09 vg/mL
5E09 vg/mL
AiE0779m_3xC2
AiE0452h_3xC2

Figure 4. Striatal enhancer AAVs maintain specificity across different delivery routes and cargos. A) Diagram of enhancer AAV vector build and range of recommended AAV dosages across stereotaxic (STX), intracerebroventricular (ICV), and retro-orbital (RO) routes of administration in mice. Note ICV delivery is in P2 pups while STX and RO are in adult mice. B-E) Representative sagittal sections of native SYFP2 fluorescence across all three delivery routes for four different enhancers targeting B-C) D1 MSNs, D) D2 MSNs, and E) cholinergic interneurons. F) Summary of detection of SYFP2 cell body expression for MSN enhancers across all three routes of administration in striatum and projection target regions. ND= none detected. G) Heatmap of on-target specificities for interneuron enhancers for the three routes of administration determined by IHC with cell type marker antibodies. H) Images of IHC comparing two cholinergic enhancers AiE0873m_3xC2 and AiE0743m_3xC2 by STX injection. White arrows show colocalization of SYFP2 and Chat. White circles in the AiE0873m_3xC2 images demonstrate off-target SYFP2 expression in MSNs. I) Diagram of enhancer AAV vector build for delivery of functional transgenes by STX injection into dorsal striatum. J) Representative sagittal images of native fluorescence for enhancer AAVs driving functional transgenes. Left: D1 MSN enhancer AiE0779m_3xC2 driving ChR2(CRC)-EYFP (AiP13278). Middle: D2 MSN enhancer AiE0452h_3xC2 driving CoChR-EGFP (AiP14035). Right: D2 MSN enhancer AiE0452h_3xC2 driving jGCaMP8m (AiP14134).

Figure 5

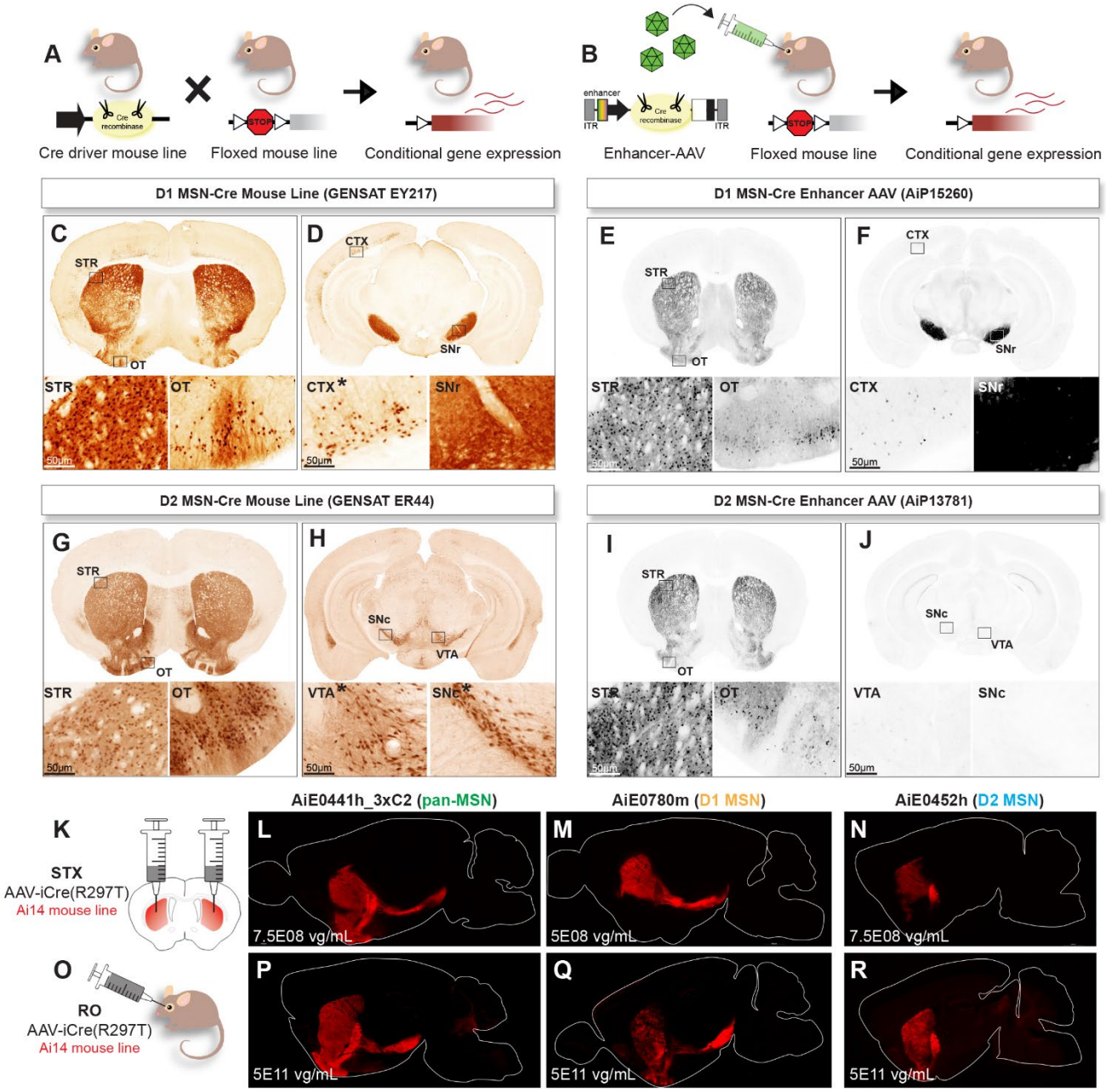

Figure 5. Comparison of D1 MSN and D2 MSN enhancer AAVs to GENSAT Cre driver lines. A) Diagram of breeding cross for generating conditional reporter transgenic mice by Cre/loxP recombination. B) Diagram of strategy for generating conditional reporter transgene expression using enhancer AAVs. C-D) ISH from www.gensat.org of GENSAT EY217 Drd1a-Cre driver line crossed to Rosa26-EGFP reporter line with C) cell body expression in striatum (STR) and islands of calleja in olfactory tubercle (OT) and D) projections to substantia nigra pars reticulata (SNr) with extra-striatal expression observed in cortex. E-F) STPT of D1 MSN enhancer AiE0779m driving iCre recombinase point mutant R297T (AiP15260) injected into Ai14 reporter mouse line with E) cell body expression in STR but not islands of calleja of the olfactory tubercle (OT) and F) projections to SNr. G-H) ISH from www.gensat.org of GENSAT ER44 Drd2-Cre driver line crossed to Rosa26-EGFP reporter line with G) cell body expression in STR but not islands of calleja in OT and H) extra-striatal dopamine neuron expression in ventral tegmental area (VTA) and SNr. I-J) STPT of D2 MSN enhancer AiE0452h driving iCre recombinase point mutant R297T (AiP13781) into Ai14 reporter mouse line with I) cell body expression in STR but not islands of calleja in OT and J) no off-target midbrain dopamine expression. K-R) Example sagittal sections of enhancer AAVs driving iCre(R297T) (AiP14825, AiP15578, and AiP13781) in Ai14 reporter mouse line either through STX (K-N) or RO (O-R) injection.

Figure 6

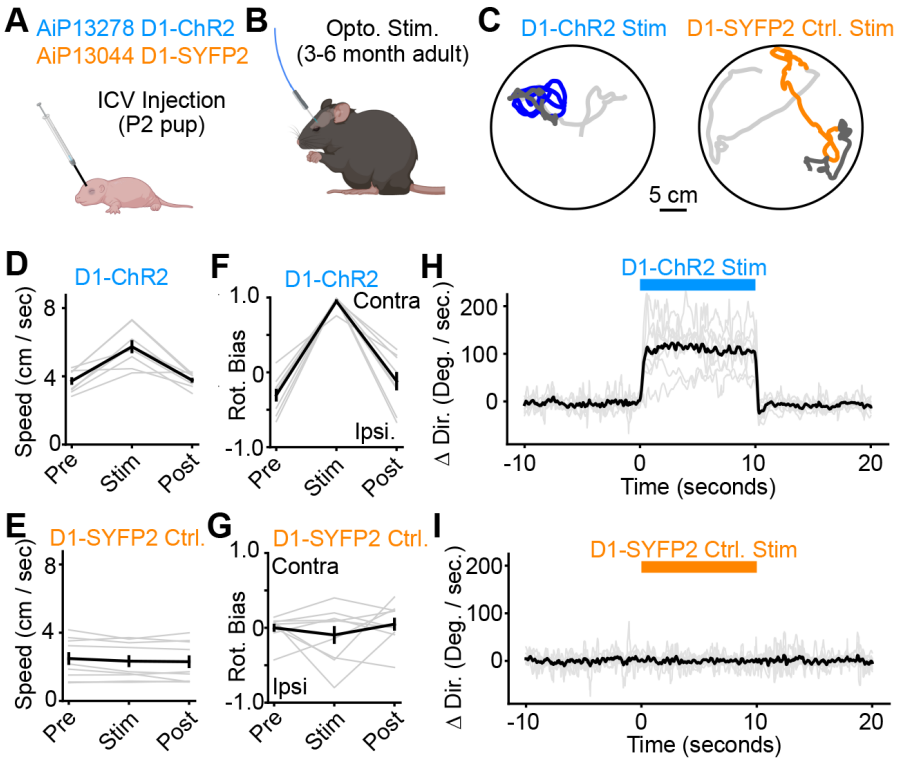

Figure 6. Optogenetic stimulation with viral vector targeting D1 MSNs is sufficient to induce locomotion and contralateral rotations. A-B) Experimental design with ICV injection of AAV vectors (AiP13278 and AiP13044, 3.0E+10 vg each) into postnatal day 2 (P2) mouse pups. Optogenetic stimulation and behavioral tracking is performed at least 1 week after stereotaxic implantation of optical fibers in adult mice. C) Exemplar tracks of mouse locomotion before (light gray; 10 sec), during (blue, orange; 10 sec), and after (dark gray; 10 sec) optogenetic stimulation in a 30 cm circular arena. D-E) Unilateral light delivery through the optical fiber (450 nm, 0.3 mW, 10 sec) increased the locomotion speed in D1-ChR2-injected mice ($p=0.0014$ pre vs. stim; 0.0016 stim vs. post; n=8 mice) but not D1-SYFP2 controls ($p=0.78$ pre vs. stim; $p=0.95$ stim vs. post; n=9 mice). F-G) Unilateral light delivery increased rotation bias towards contralateral rotations in D1-ChR2 injected mice ($p<10\text{-}6$ pre vs. stim; $p<10\text{-}4$ stim vs. post; n=8 mice) but not D1-SYFP2 control mice ($p=0.50$ pre vs. stim; $p=0.37$ stim vs. post; n=9 mice). H-I) Optogenetic stimulation induced steady contralateral rotations within ~200 ms of the onset of light stimulation in D1-ChR2-injected mice but not SYFP2 controls. Rotations persisted throughout the stimulation. All p values reflect unpaired t-test with unequal variance.

Figure 7

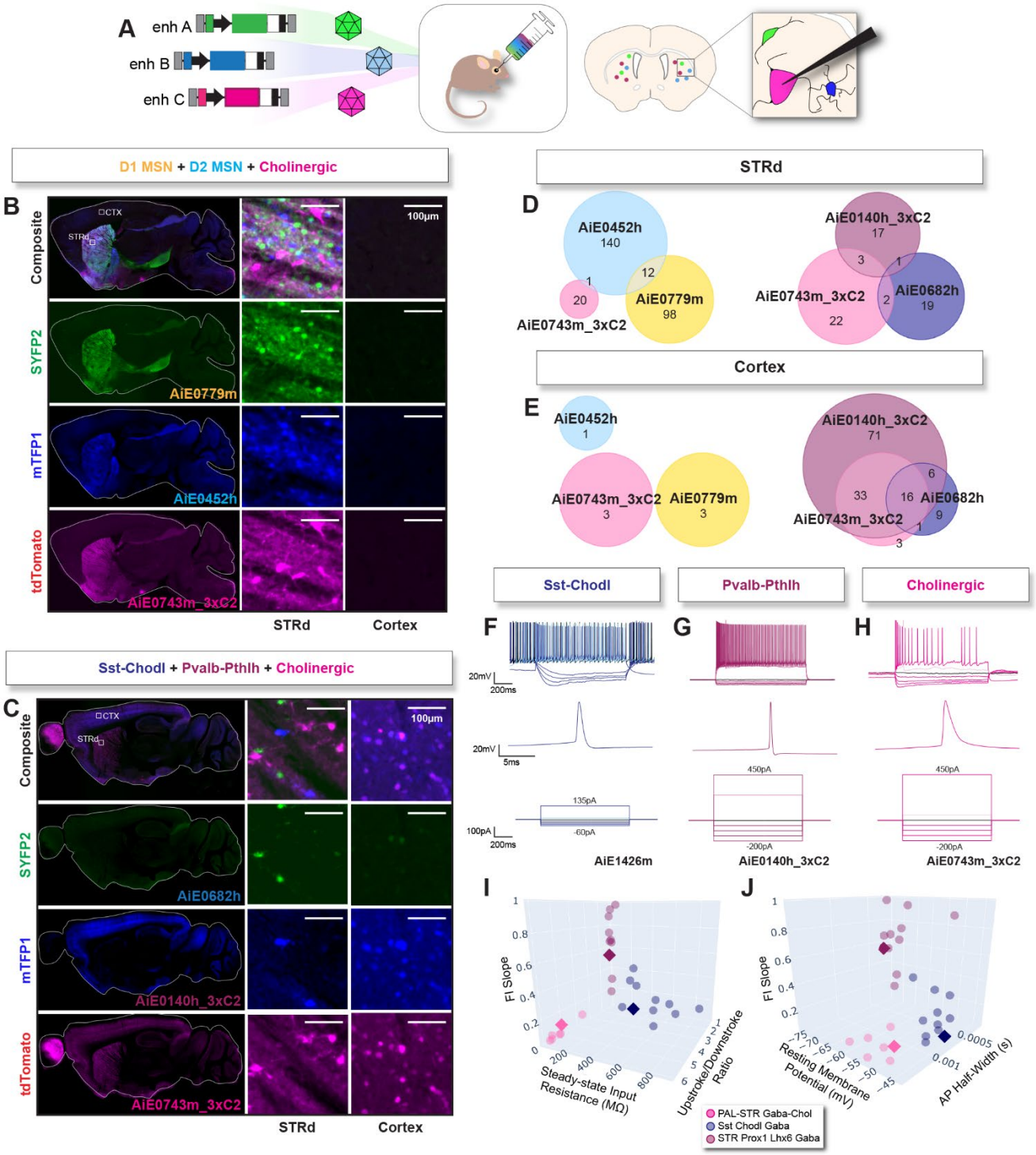
A
enh A
enh B
enh C
D1 MSN + D2 MSN + Cholinergic
B
Composite
SYFP2
mTFP1
tdTomato
CTX
STRd
100µm
AiE0779m
AiE0452h
AiE0743m_3xC2
STRd
Cortex
Sst-Chodl + Pvalb-Pthlh + Cholinergic
C
AiE0682h
AiE0140h_3xC2
STRd
Cortex
STRd
D
AiE0452h
140
12
1
20
AiE0779m
98
AiE0743m_3xC2
AiE0140h_3xC2
17
3
1
AiE0743m_3xC2
2
AiE0682h
19
22
Cortex
E
AiE0452h
1
AiE0743m_3xC2
3
AiE0779m
3
AiE0140h_3xC2
71
6
33
16
AiE0682h
AiE0743m_3xC2
9
1
3
Sst-Chodl
Pvalb-Pthlh
Cholinergic
F
G
H
20mV
200ms
20mV
5ms
135pA
-60pA
100pA
200ms
450pA
-200pA
450pA
-200pA
AiE1426m
AiE0140h_3xC2
AiE0743m_3xC2
I
J
FI Slope
Steady-state Input Resistance (MΩ)
Upstroke/Downstroke Ratio
Resting Membrane Potential (mV)
AP Half-Width (s)
PAL-STR Gaba-Chol
Sst Chodl Gaba
STR Prox1 Lhx6 Gaba

Figure 7. Concurrent striatal cell type identification by multiplexed enhancer AAV delivery. A) Enhancer AAVs were individually packaged, pooled, and injected RO into adult mice. Enhancer-driven fluorescence was used to identify striatal cell types for patch clamp recordings. B) Example sagittal sections of triple labeling using D1 MSN enhancer AiE0779m driving SYFP2 (AiP12609), D2 MSN enhancer AiE0452h driving mTFP1 (AiP12700), and cholinergic interneuron enhancer (AiE0743m_3xC2) driving tdTomato (AiP13738). Zoomed in views of dorsal striatum (STRd, middle) and cortex (right). C) Example sagittal sections of triple labeling using striatal Sst-Chodl enhancer (AiE0682h) driving SYFP2 (AiP12689), Pvalb-Pthlh enhancer (AiE0140h_3xC2) driving mTFP1 (AiP13808), and cholinergic enhancer (AiE0743m_3xC2) driving tdTomato (AiP13738). Zoomed in views of dorsal striatum (STRd, middle) and cortex (right). Note off-target tdTomato expression in cortex from AiE0743m_3xC2. D-E) Quantification of both multiplex injection combinations in dorsal striatum (D) and cortex (E). Numbers in Venn diagrams represent cell counts for each enhancer driven fluorescent reporter. F-H) Single cell patch clamp recordings from coronal brain slices derived from a mouse with multiplex injection of F) Sst-Chodl enhancer AiE1426m-SYFP2 (AiP15050), G) Pvalb-Pthlh enhancer AiE0140h_3xC2-mTFP1 (AiP13808), and H) Cholinergic enhancer AiE0743m_3xC2-tdTomato (AiP13738). Top: Representative voltage traces of responses (mV) to hyperpolarizing and depolarizing current steps (pA). Trace in the lightest shade shows firing pattern after first current step to reach threshold and elicit firing. Note characteristics that distinguish each cell type: prominent sag for Sst-Chodl, high firing rate for Pvalb-Pthlh, and spontaneous firing for cholinergic interneurons. Middle: Example action potential trace for each cell type. Bottom: Current steps used to generate recordings. Line in lightest shade was current step used to reach threshold and elicit firing. I-J) 3D plots comparing electrophysiological features that distinguish the three striatal interneuron types. I) Comparison of the slope of the FI (frequency/current) curve (voltage responses as a function of hyperpolarizing and depolarizing current applied), the steady state input resistance (linear fit of the current-voltage relationship in response to hyperpolarizing current steps), and action potential upstroke and downstroke ratio. J) Comparison of the slope of the FI curve with the resting membrane potential and the action potential half-width.

Figure 8

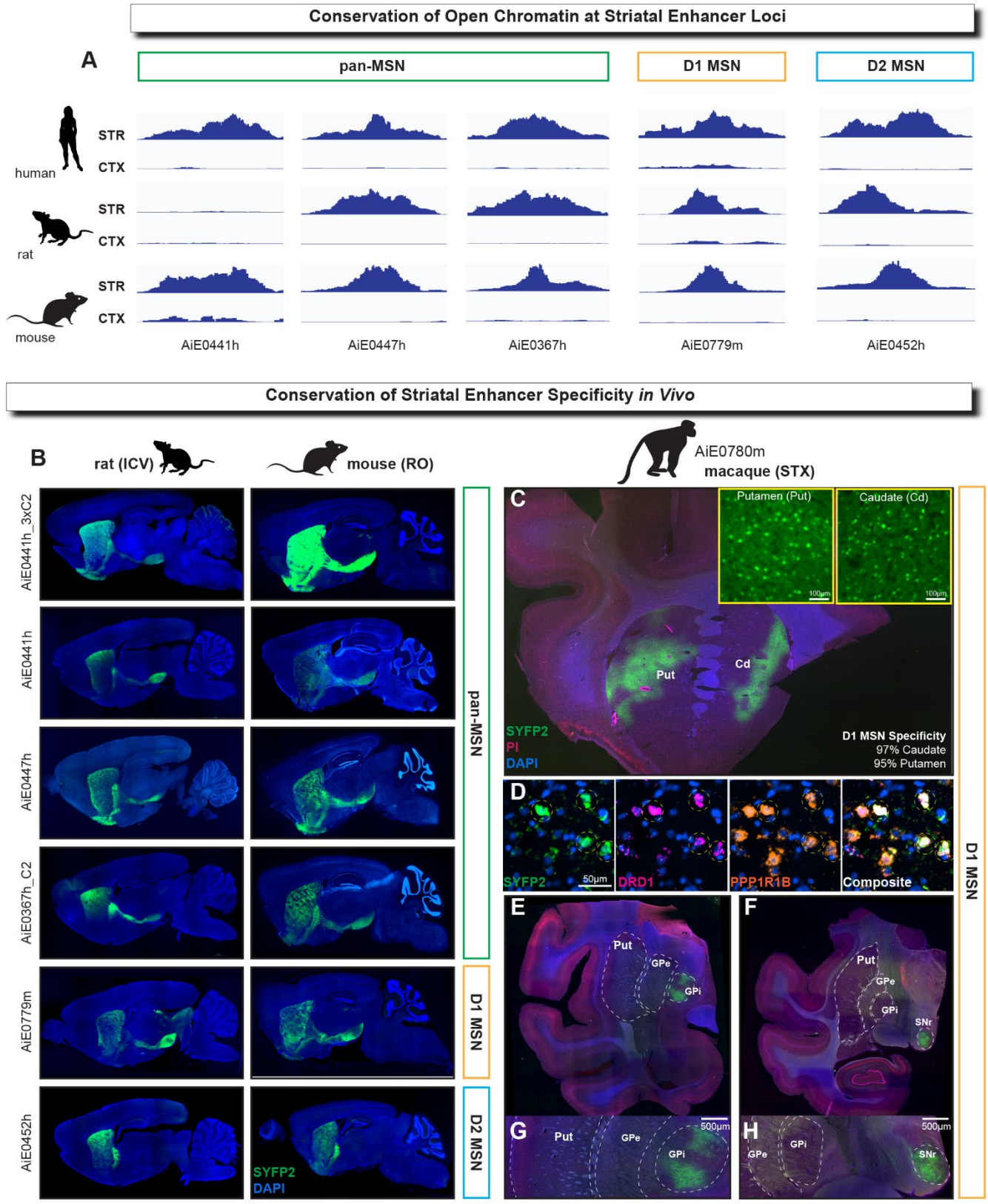
Conservation of Open Chromatin at Striatal Enhancer Loci
A
pan-MSN
D1 MSN
D2 MSN
human
rat
mouse
STR
CTX
AiE0441h
AiE0447h
AiE0367h
AiE0779m
AiE0452h
Conservation of Striatal Enhancer Specificity in Vivo
B
rat (ICV)
mouse (RO)
AiE0441h_3xC2
AiE0441h
AiE0447h
AiE0367h_C2
AiE0779m
AiE0452h
SYFP2
DAPI
pan-MSN
D1 MSN
D2 MSN
AiE0780m
macaque (STX)
C
Putamen (Put)
Caudate (Cd)
100µm
Put
Cd
SYFP2
PI
DAPI
D1 MSN Specificity
97% Caudate
95% Putamen
D
SYFP2
50µm
DRD1
PPP1R1B
Composite
E
F
Put
GPe
GPi
SNr
G
H
500µm
D1 MSN

Figure 8. Cross-species conservation of striatal enhancer open chromatin and enhancer AAV activity *in vivo*. A) Assessment of evolutionary conservation of open chromatin activity. Bulk ATAC-seq analysis showing open chromatin regions in the cortex and striatum of human, rat, and mouse at conserved orthologs of five selected enhancer loci. These enhancers include three pan-MSN enhancers, one D1 MSN enhancer, and one D2 MSN enhancer. ATAC-seq traces demonstrate conserved higher open chromatin activity in the striatum compared to the cortex for all enhancers except the ortholog of AiE0441h in rat, which shows no chromatin accessibility in either cortex or striatum. B-H) Conservation of striatal enhancer specificity *in vivo*. B) Enhancer AAVs corresponding to the set of enhancers shown in (A), including an additional optimized variant (AiE0441h_3xC2), were injected RO into mouse and ICV into rat. Sagittal brain sections show conserved patterns of enhancer activity in mouse versus rat brain for native SYFP2 fluorescence (green), with DAPI counterstain (blue). Images were not acquired under matched conditions and have been adjusted to optimally highlight brain wide expression patterns for enhancer specificity comparison purposes. C-H) Stereotaxic injection of AiE0780m driving SYFP2 (AiP12610) in macaque caudate and putamen using a BrainSight Robot. C) Coronal section of striatum injection site with red=propidium iodide, blue=DAPI, green=native SYFP2. Insets of caudate (cd) and putamen (put) show native SYFP2 only. D) Example images of RNAscope from Putamen injection site. E-H) Coronal sections posterior to the injection site showing axon projections through the GPi and SNr indicative of D1 MSNs with red=propidium iodide, blue=DAPI, green=native SYFP2.